

## A simple running model with rolling contact and its role as a template for dynamic locomotion on a hexapod robot

This content has been downloaded from IOPscience. Please scroll down to see the full text.

2014 Bioinspir. Biomim. 9 046004

(<http://iopscience.iop.org/1748-3190/9/4/046004>)

View [the table of contents for this issue](#), or go to the [journal homepage](#) for more

### Download details:

This content was downloaded by: peichunlin

IP Address: 140.112.14.18

This content was downloaded on 08/10/2014 at 00:44

Please note that [terms and conditions apply](#).

# A simple running model with rolling contact and its role as a template for dynamic locomotion on a hexapod robot

Ke-Jung Huang<sup>1</sup>, Chun-Kai Huang<sup>1</sup> and Pei-Chun Lin

Department of Mechanical Engineering, National Taiwan University, Taipei, Taiwan

E-mail: [peichunlin@ntu.edu.tw](mailto:peichunlin@ntu.edu.tw)


Received 24 November 2013, revised 17 July 2014

Accepted for publication 23 July 2014

Published 7 October 2014

## Abstract

We report on the development of a robot's dynamic locomotion based on a template which fits the robot's natural dynamics. The developed template is a low degree-of-freedom planar model for running with rolling contact, which we call rolling spring loaded inverted pendulum (R-SLIP). Originating from a reduced-order model of the RHex-style robot with compliant circular legs, the R-SLIP model also acts as the template for general dynamic running. The model has a torsional spring and a large circular arc as the distributed foot, so during locomotion it rolls on the ground with varied equivalent linear stiffness. This differs from the well-known spring loaded inverted pendulum (SLIP) model with fixed stiffness and ground contact points. Through dimensionless steps-to-fall and return map analysis, within a wide range of parameter spaces, the R-SLIP model is revealed to have self-stable gaits and a larger stability region than that of the SLIP model. The R-SLIP model is then embedded as the reduced-order 'template' in a more complex 'anchor', the RHex-style robot, via various mapping definitions between the template and the anchor. Experimental validation confirms that by merely deploying the stable running gaits of the R-SLIP model on the empirical robot with simple open-loop control strategy, the robot can easily initiate its dynamic running behaviors with a flight phase and can move with similar body state profiles to those of the model, in all five testing speeds. The robot, embedded with the SLIP model but performing walking locomotion, further confirms the importance of finding an adequate template of the robot for dynamic locomotion.

 Online supplementary data available from [stacks.iop.org/BB/9/046004/mmedia](http://stacks.iop.org/BB/9/046004/mmedia)

Keywords: SLIP, rolling contact, legged robot, dynamic locomotion, reduced-order model

(Some figures may appear in colour only in the online journal)

## 1. Introduction

The natural environment is usually rough and varied. Most ground animals have evolved with agile and robust legs which allow them to move gracefully and swiftly across uneven terrain. Though the geometrical configurations and evolved stages of the legs may vary significantly, researchers have found that, through adequate motion coordination among the legs, an animal's dynamic locomotion in the

sagittal plane can be approximated by a simple mathematical model: (spring loaded inverted pendulum (SLIP) [1–3]. Here the body is treated as a point mass and the legs are approximated by a massless linear spring. The SLIP model is energy conservative, and is widely recognized as the intrinsic and qualitative representation of ground animals' running behavior. As a running 'template', the SLIP model indeed provides a prescriptive control guide to the original complex biological systems which represent empirical 'anchors' by sketching the actuation joints and rigid structures [4]. Consequently, the past few decades' successful development of

<sup>1</sup> These two authors contributed equally.

legged robots with dynamic behavior is basically judged by the similarity of the robots' locomotion characteristics to that of the SLIP model. More specifically, the robot should have a flight phase as well as an alternating energy exchange between potential and kinetic energies during locomotion.

The study of dynamic robotic systems was initiated by the development of monopods in the 1980s [5]. Following this, various quadruped and hexapod robots with dynamic behaviors were reported early in the millennium. Examples include the Scout series [6, 7], Tekken series [8, 9], Sprawl series [10–12], and RHex [13–16]. In addition, a dynamic climbing robot has been reported [17]. Possibly owing to the limited power density of commercial motors, excitation of the dynamic behaviors of these robots relies mostly on adequate allocation of compliant parts as well as coordination of these parts with the active joint motion, so that the potential energy of the spring can be transferred to and from the kinetic energy of the system. For example, the hexapod iSprawl has carefully tuned leg compliance. It can be driven by a single motor, and it generates SLIP-like locomotion [12]. The hexapod RHex has only one rotational degree of freedom (DOF) per leg, but it can generate SLIP-like jogging behavior with its compliant legs [13]. In addition, RHex can perform various interesting dynamic behaviors [18]. The recently developed BigDog, Cheetah, and WildCat robots from Boston dynamics can perform fantastic dynamic behaviors. Instead of using electric motors, the robots have high-power hydraulic systems to drive multi-DOF legs as springs; however, very little technical information has been released to the public.

In addition to the above works which focus on the dynamic behaviors of empirical robots, some works have addressed the relation between the template and the anchor. For example, Poulakakis and Grizzle introduced asymmetric SLIP to create stable running of the monopodal robot Thumper [19]. Ankarali and Saranlı used SLIP as a template to achieve stable pronking for a planar and underactuated hexapod robot, and an embedding controller as a torque-actuated model (SLIP-T) which can reveal the behavior of the hip joint motors on the RHex-style robot [20]. Koepf and Hurst treated the actuated spring-mass system as a force-controlled actuator and commanded forces according to the passive dynamics of the ideal SLIP model [21]. Hutter *et al* utilized an operational space controller that imposed the SLIP dynamics onto an actual segmented robotic leg [22]. The above works address the problem with analytic or numerical approaches on a very deep and detailed level. Only the last work includes experimental results, yet the mapping is from the one-leg template (i.e., the SLIP model) to the one-leg articulated leg, not from the one-leg template to the whole multi-legged robot.

Here, aiming at developing dynamic behaviors for a multi-legged robot based on the template, we take the robot's characteristics as the prior constraints and search for its natural dynamics as the right template. We then seek an adequate mapping between this template and the multi-legged robot. The RHex-style robot is utilized as the experimental platform because of its simple mechanical structure yet agile mobility. Although the early versions of the RHex used four-bar Delrin legs because of their similar performance to a linear spring, in later versions half-circular legs were utilized for their

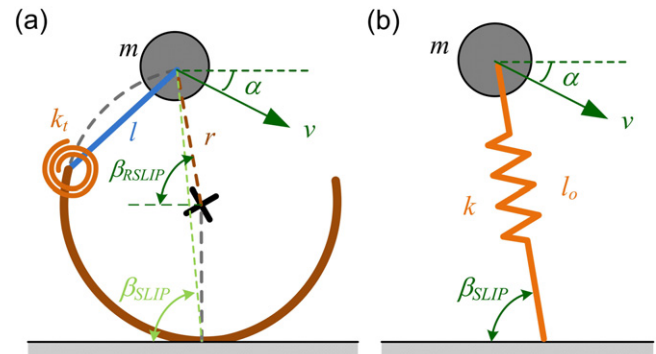


**Figure 1.** Model sketches and parameters: (a) the R-SLIP model and (b) the SLIP model.

robustness and dynamic performance [23, 24]. The half-circular morphology is utilized in other RHex variations as well [25, 26]. However, the half-circular leg has two distinct performance characteristics which differ from the ideal linear spring. First, the linear spring ideally has a fixed ground contact point, in contrast to the half-circular leg which rolls on the ground so that the ground contact point keeps moving forward. This behavior is at some level equal to shifting the center of pressure forward within stride, similar to a human running with his center of pressure moving from the posterior to the anterior of the foot [27]. Flex-Foot Cheetah, a prosthetic human foot worn by amputee athletes, also has rolling contact with the ground. In addition, the rolling behavior endows the whole half-circular leg as a distributed foot, which provides greater mobility [28]. The second difference is that, owing to the forward movement of the ground contact point, equivalent linear stiffness of the half-circular leg changes as it rolls on the ground. As a result, the linear spring may not be a good model for the robot with half-circular legs, which means the SLIP model may not be the right template for the RHex-style robot with half-circular legs.

We propose a new SLIP model which has intrinsic properties of rolling behavior and variable stiffness as shown in figure 1(a) and is hereafter referred to as rolling spring loaded inverted pendulum (R-SLIP). Its configuration is inspired from the compliant behavior of thin half-circular material, based on analysis of solid mechanics. Basically, the R-SLIP model is composed of a large circular rolling foot, a short bar with a point mass on top, and a torsion spring connecting the other end of the short bar and one end of the rolling foot. The large circular foot can adequately model the rolling behavior of the circular leg. While the R-SLIP model rolls on the ground, equivalent linear compliance of the model changes because the distance between the ground contact point and the torsion spring changes simultaneously (i.e., its moment arm is changing). As a result, the two characteristics of the circular leg in the previous paragraph can be preserved in the proposed reduced-order R-SLIP model.

Though the R-SLIP model originated from an understanding of the dynamic behavior of the circular leg, in which this specific type of leg permits RHex to exhibit a rich set of dynamic behaviors, the R-SLIP model itself acts as a novel reduced-order model and can serve as the template for a

legged system with dynamic locomotion. Owing to its novel configuration, it has dynamic characteristics that are different from other recently-developed reduced-order models. Rummel *et al* proposed a two-segment model with point ground contact and variable equivalent linear stiffness, and the model has larger stability than the ordinary SLIP [29]. Jun and Clark reported a SLIP model with fixed linear stiffness and a rolling foot (SLIP-R) which confirmed that the rolling foot increases the region of stable gaits [30]. Ankarali *et al* proposed a C-Pod model with a half-circle shape [31]. While the model rolls on the ground, its equivalent linear stiffness varies, and the quantitative computation of its dynamic behavior is based on the assumption that the model maintains a circular shape and fixed arc length. In addition, some recent models have energy input and dissipation elements. For example, Seipel and Holmes proposed a lossy clock-torqued SLIP [32], and later Shen and Seipel discussed the fundamental mechanism of the SLIP model with hip torque and leg damping [33]. Jun and Clark reported a torque-driven and damped half-circle-leg model, where the rolling contact of the circular leg is modeled as a sequential change of two-segment legs [34].

The contribution of this work lies in two aspects: one is the methodology of developing dynamic behaviors of the robot based on the template, which roughly represents the robot's natural dynamics; the other is development and analysis of the new model R-SLIP (with partial results presented in [35]). The R-SLIP model is conservative and has four intrinsic parameters (while the SLIP model has three). Owing to simplicity, dynamic behavior of the model can be investigated in a complete range of parameter spaces. In addition, because the R-SLIP model is inspired from the mechanics of empirical half-circular legs, its dynamic behavior approximates that of the original complex system. Thus, by establishing an adequate mapping between the R-SLIP model and the robot, the dynamic behavior of the robot can easily be initiated, completing the control structure formed by template and anchor [4]. As a result, the methodology used in this work is neither merely model development nor an attempt to make the existing robot act like an ordinary SLIP, but to investigate the adequate template for the existing robot, followed by linking the dynamic behaviors between the simple template and the original complex robot.

Section 2 describes generation of the R-SLIP model through the solid mechanics analysis of the half-circular material. Section 3 reports the quantitative formulation of the dynamic R-SLIP model. Section 4 provides some detailed consideration for model analysis, including the setup for comparing performance with the SLIP model. Sections 5 and 6 report the results of steps-to-fall and return map analysis, respectively. Section 7 describes the methodology of using R-SLIP as the template for dynamic behavior initiation on the RHex-style hexapod robot. Section 8 concludes the work.

## 2. Origination of the R-SLIP model

The design concept of the R-SLIP model is based on the SLIP model, which is composed of a point mass and a massless

compliant leg. However, instead of having a linear spring with point-contact to the ground as the 'virtual leg', the R-SLIP has a torsional spring and a circular leg for rolling contact. The formulation of the R-SLIP model originated from the mechanics of the thin circular-shape compliant material, described in detail below.

The material in a half-circular shape is provided as the illustrative example. Assume that a massless, elastic, isotropic, and half-circular material is fixed at one end,  $P_H$ , and is under force  $F = [F_h \ F_v]^T$  at the other end,  $P_E$ , which has a horizontal component,  $F_h$  and a vertical component  $F_v$  as shown in figure 2(a). Then, as shown in figure 2(b) the moment at an arbitrary position  $P_a$  on the half-circular material can be represented as

$$M_b(\theta) = r(F_v \sin(\theta) - F_h(1 - \cos(\theta))), \quad (1)$$

where  $\theta$  is the angle included by the line segments  $OP_a$  and  $OP_E$ . The strain energy of the deformed half-circular material,  $U$ , can be expressed as

$$U = \int_{P_E}^{P_H} \frac{M^2}{2EI} ds = \int_0^\pi \frac{M_b(\theta)^2}{2EI} r d\theta, \quad (2)$$

where the energy from normal stress and shear stress is ignored because they are relatively small in comparison to that of bending. The horizontal displacement,  $\delta h$ , and vertical displacement,  $\delta v$ , of the position  $P_E$  can be expressed as

$$\begin{aligned} \delta h &= \frac{\partial U}{\partial F_h} = \frac{3\pi r^3}{2EI} F_h - \frac{2r^3}{EI} F_v, \\ \delta v &= \frac{\partial U}{\partial F_v} = -\frac{2r^3}{EI} F_h + \frac{\pi r^3}{2EI} F_v. \end{aligned} \quad (3)$$

Equation (3) can further be formatted in the matrix representation

$$\begin{aligned} D &= \begin{bmatrix} \delta h \\ \delta v \end{bmatrix} \\ &= \frac{r^3}{2EI} \begin{bmatrix} 3\pi & -4 \\ -4 & \pi \end{bmatrix} \begin{bmatrix} F_h \\ F_v \end{bmatrix} \\ &= M_c F, \end{aligned} \quad (4)$$

with  $M_c$  being the compliance matrix (i.e., inverse of the stiffness matrix). The matrix is diagonalizable and can be represented as

$$M_c = SAS^{-1}, \quad (5)$$

where the matrix  $S$  is formed by eigenvectors of  $M_c$  and the diagonal matrix  $\Lambda$  is the principal compliance matrix, formed by corresponding eigenvalues. Thus, the principal stiffness matrix,  $\Lambda^{-1}$ , can be derived as

$$\Lambda^{-1} = S^{-1}M_c^{-1}S, \quad (6)$$

and its numerical approximation is

$$\Lambda^{-1} = \frac{2EI}{r^3} \begin{bmatrix} 0.84 & 0 \\ 0 & 0.09 \end{bmatrix}. \quad (7)$$

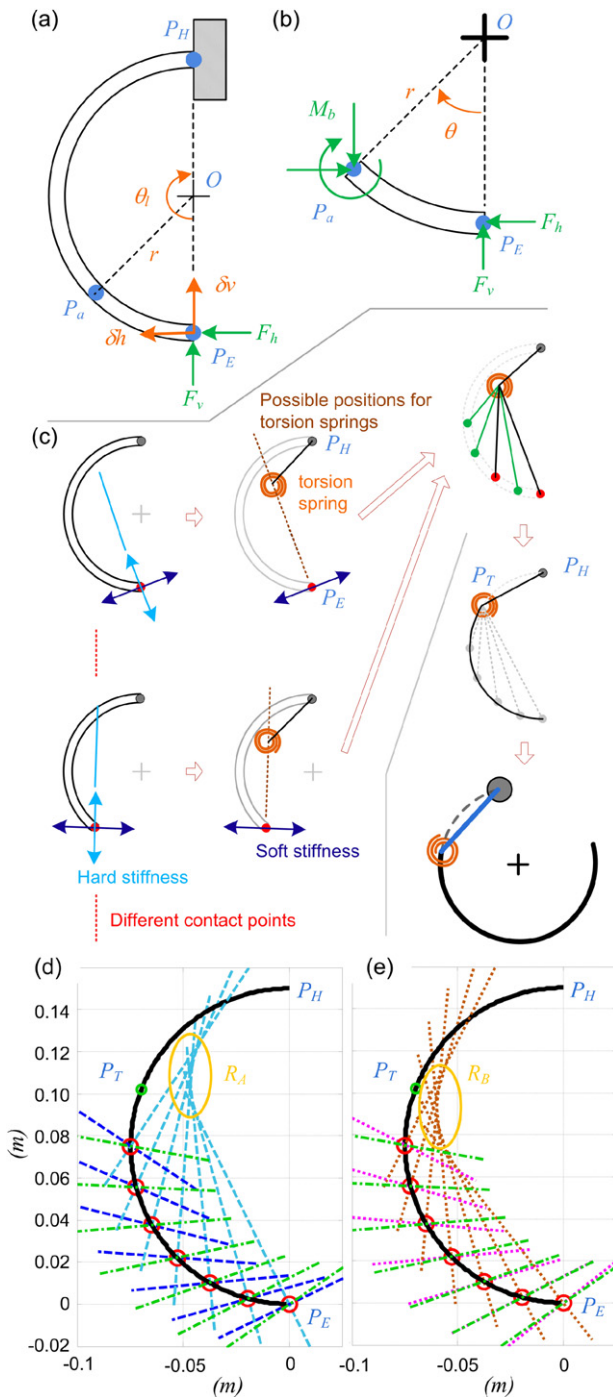


**Figure 2.** The compliant property of the thin, massless, elastic, isotropic, and half-circular material. (a) Boundary conditions: one fixed end at  $P_H$  and one forced end at  $P_E$ . (b) Free body diagram of the arbitrary arc section  $P_a P_E$ . (c) Modeling stiffness characteristics of the half-circular material by a reduced-order model with a torsion spring. (d) The directions of the principal stiffness axes of the stiffness matrices while the forces are individually applied at seven different positions. The dashed blue lines and dashed cyan lines represent the directions of the soft and hard springs, respectively. (e) The dotted magenta lines represent the deformation direction when the material is applied with a force along the direction toward point  $P_H$ . The dotted brown lines pass through contact points and are perpendicular to the dotted magenta lines. In both (d) and (e), the dash-dotted green lines represent the deformation directions of the R-SLIP model with a torsion spring mounted at  $P_T$ .

Note that the numbers in the matrix shown in (7) are determined purely by geometrical configuration, and are not related to material properties since the latter are located outside of the matrix.

The eigendecomposition process described in (6) reveals two principal deformation directions of the half-circular material (i.e., the directions of the ‘soft spring’ and the ‘hard spring’). They are sketched in figure 2(c) and plotted in figure 2(d) as the small cross which passes point  $P_E$  and is composed of a dashed blue line segment indicating the direction of the soft spring, and a dashed cyan line segment for the direction of the hard spring, respectively. The diagonal matrix shown in (7) indicates that the stiffness along the direction of the hard spring is close to an order of magnitude greater than that of the soft spring. As a result, the half-circular material is much easier to deform along the direction of the soft spring. Thus, if the compliance along the stiffer axis is ignored and only that along the softer axis is preserved, the compliance of the material can be simulated by a system composed of a torsion spring, mounted at some point on the stiffer axis, and two rigid links. One link connects the torsion spring and the fixed point,  $P_H$ , and the other link connects the spring and the ground contact point,  $P_E$ , as shown in figure 2(c).

The principle stiffness matrices of the material while under force at different positions are investigated as well because the half-circular material ( $\theta_l = 180^\circ$ ) may contact the ground at different positions (i.e., rolling contact) when it is utilized as the virtual leg of the model. This can be done by using the same method but with different integration ranges shown in (2) and coordination rotations. The results are shown in table 1 and figure 2(d). Table 1 lists the stiffness of the soft ( $k_s$ ) and hard ( $k_h$ ) springs along the principal axes while the forces are individually applied at seven different positions (i.e., at red circles,  $\theta_l = 180^\circ - 90^\circ$ ). Their corresponding directions are plotted in figure 2(d). Note that the numbers listed in the table are the diagonal components of the matrix shown in (7). The absolute values of the stiffness are the listed numbers multiplied by  $2EI/r^3$ . Because the latter are the same in the virtual leg, only the ‘scaling’ parts are listed.

Table 1 and figure 2(d) provide useful hints to design a reduced-order model based on the characteristics of the half-circular material. First, the stiffness changes when the contact point changes. This phenomenon indicates that when the material rolls on the ground, the shorter the material (i.e., with the contact point moving up, closer to the top of the material), the greater its stiffness. Second, the effect of the harder spring may be ignored because in almost all cases the hard springs are at least an order of magnitude stiffer than the soft springs. Thus, the simplified model can also be constructed for the material with different contact points as shown in figure 2(c). In addition, the directions of the hard springs (i.e., dashed cyan line segments shown in figure 2(d)) roughly intersect with each other around the upper portion of the material (i.e., region  $R_A$ ). This characteristic further suggests that a torsion spring placed around region  $R_A$  is adequate for the material with different contact points.

**Table 1.** Stiffness of the circular material along with the principal axes.

$\theta_t$	180	165	150	135	120	105	90
$k_s$	0.09	0.10	0.13	0.16	0.21	0.30	0.45
$k_h$	0.84	1.19	1.79	2.85	4.86	9.03	18.74
$k_h/k_s$	9.49	11.51	14.18	17.81	22.90	30.32	41.77

**Table 2.** Stiffness characteristics of the half-circular material and the R-SLIP model.

$\theta_t$	180	165	150	135	120	105	90
$k_s/k_{s,180}$	1	1.18	1.44	1.82	2.42	3.39	5.10
$k_t/k_{t,180}$	1	1.11	1.27	1.51	1.91	2.67	4.52
$ \delta $ ( $^\circ$ )	-3.6	-0.1	3.3	6.6	9.9	13.1	16.2

When the half-circular material is used as a massless leg of a conservative reduced-order model, the force at the contact point is along the direction toward point  $P_H$ , and the resultant deformation directions of the material (dotted magenta line segments) can be derived by taking effects from both the soft and hard springs as shown in figure 2(e). By using the same analogy of the torsion spring as described in the previous paragraphs, the region intersected by the dotted brown lines which pass through the contact points and are perpendicular to these resultant deformation directions are intersected with each other around the upper portion of the material (i.e., region  $R_B$ ). This characteristic also suggests that a torsion spring placed around region  $R_B$  is adequate for the material with different contact points.

Owing to the proximity of  $R_A$  and  $R_B$  to the circular rim, the torsion spring of the final reduced-order model is set to locate at  $P_T$ , on the circular rim as shown in figure 2(c). By doing so, the geometric parameters needed to define the model can be reduced by one. As a result, the compliant behavior of the half-circular material with different contact points (shown as red circles) can be simulated by a model composed of a torsion spring at  $P_T$ , a link connecting the spring to the fixed point  $P_H$ , and rigid links connecting the spring and the red points. The links can be further replaced by a rigid circular arc which connects the torsion spring and the ground contact points, with the circular arc length extended beyond point  $P_E$  to prevent point-contact behavior when the leg rolls to the end of the arc. Further, because the shape of the link  $P_T P_H$  connecting the torsion spring at  $P_T$  to the fixed point  $P_H$  is not important, a straight link is utilized. Finally, by adding a point mass at  $P_H$ , a simplified reduced-order and spring-mass model has the configuration shown in figure 1(a), and is named R-SLIP.

The qualitative behavior of the R-SLIP model is similar to that of the compliant half-circular leg. When the R-SLIP model rolls on the ground, the ground-contact point moves forward as the circular leg does. In the meantime, because the distance between the ground-contact point and the torsion spring changes accordingly, the equivalent linear stiffness between the mass and ground contact point varies. Therefore, the compliance change in the circular leg during locomotion can be captured in the R-SLIP model as well. Table 2 lists the stiffness trends of the half-circular material and the R-SLIP model. The symbols  $k_s$  and  $k_t$  indicate the stiffness of the material and R-SLIP, respectively. The stiffness data is normalized by the stiffness at which the contact point is located at  $P_E$  (i.e., with subscript, 180). The table also lists the

absolute difference of the deformation directions between the material and the model,  $|\delta|$ , and these two directions are plotted in figure 2(e) as well (dotted magenta line segments and dash-dotted green line segments). The stiffness increasing trends of the model is less than that of the material, and in most occasions the percentage error is less than 20%. In addition, the absolute deformation direction differences are less than  $10^\circ$  when the leg rolls at the lowest one third of the leg. In summary, the quantitative characteristics of the half-circular material can be captured by the R-SLIP model in a reasonable manner.

Note that though the morphology of the R-SLIP model is originated from the behavior of the half-circular material, the main purpose of developing the R-SLIP model is not to merely find a model whose behavior is accurately matched to the half-circular material, but to define a general template with the following characteristics: (i) having rolling behavior; (ii) having as few parameters as possible; (iii) providing the abstract model which can represent the compliant rolling material as closely as possible. From this aspect, the simplification by relocating the torsion spring on the circular rim is quite important. The number of parameters of the R-SLIP model in the present form is four, one more than the SLIP model. Owing to the low parameter number, we are able to do the model analysis as completely as possible and to compare its behavior to the SLIP model in a fair manner.

### 3. Formulation of the R-SLIP dynamic model

Figure 1(a) depicts the composition of the R-SLIP model. It has two segments connected by a torsion spring. The lower rigid segment is part of a circular rim, thus performing rolling behavior during its ground contact period. The spring constant of the torsion spring is assumed to be fixed, which is easier for analysis and simulation. The upper rigid link connects the torsion spring and a point mass. When the spring is in its natural configuration, the mass is located on the circular rim as well (i.e., with the same distance to the center of the circular rim as the radius of the circular rim). Therefore, the R-SLIP model has four intrinsic parameters: radius of the circular rim ( $r$ ), stiffness of the torsional spring ( $k_t$ ), mass ( $m$ ), and distance between the torsion spring and the mass ( $l$ ). In contrast, the SLIP model has three parameters: length of spring, stiffness of spring, and mass as shown in figure 1(b).

Similar to the SLIP model, a full running stride of the R-SLIP model can be divided into stance phase and flight phase

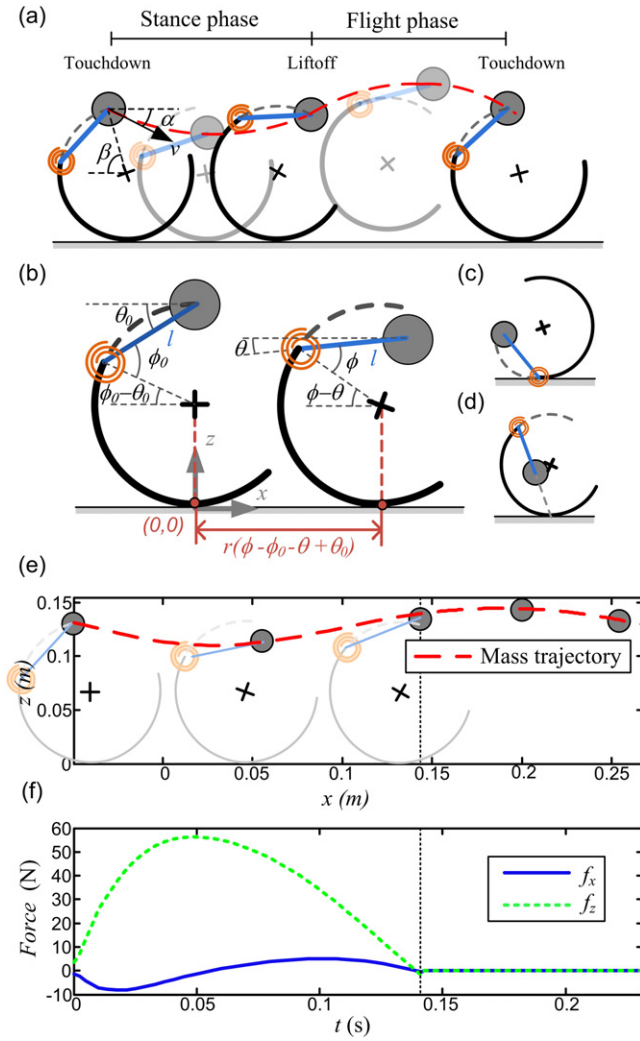


**Figure 3.** The R-SLIP model: (a) Illustrative sketch of its running motion with stance phase and flight phase. The variables for defining the touchdown state are also presented. (b) The parameters utilized in the development of the modified SLIP model. (c), (d) Two extreme conditions where the numerical simulation of the R-SLIP model fails. (e) Trajectory and (f) ground reaction force of the R-SLIP model during locomotion.

as shown in figure 3(a). In flight phase, the R-SLIP model moves according to the ballistic model, where the forward motion is at constant speed and the vertical motion is affected by gravity. With a pre-determined landing angle  $\beta$ , touchdown occurs and the stance phase begins when the height of the mass to the ground is less than  $r + r \sin(\beta)$ . Owing to the landing momentum, the R-SLIP model rolls on the ground and the torsion spring is simultaneously compressed. At a certain moment the spring starts uncompressing. Right after the torsion spring returns to its natural configuration, the R-SLIP model lifts off and the flight phase begins. If the R-SLIP model moves stably, its motion is composed of these two phases alternating periodically.

The quantitative dynamic behavior of the R-SLIP model in stance phase can be investigated by constructing its dynamic model by the Lagrangian method. The angles  $\theta$  and

$\phi$  are utilized as the generalized coordinates as depicted in figure 3(b). The angle  $\theta$  is defined as the angle included by the horizontal line and the line segment connecting the torsion spring and the mass,  $l$ . The angle  $\phi$  represents the compression level of the torsion spring, and is defined as the angle included by  $l$  and the line connecting the torsion spring and the center of the circular rim. Following these definitions, the Cartesian coordinates of the mass in the stance phase,  $(x_s, z_s)$ , can be represented as

$$\begin{bmatrix} x_s \\ z_s \end{bmatrix} = \begin{bmatrix} r(\phi - \phi_0 - \theta + \theta_0) - r \cos(\phi - \theta) + l \cos \theta \\ r + r \sin(\phi - \theta) + l \sin \theta \end{bmatrix}, \quad (8)$$

where the subscripts  $s$  of  $(x, z)$  and 0 of  $\theta$  and  $\phi$  indicate the stance phase and natural configuration, respectively. The kinetic energy,  $T$ , and potential energy,  $V$ , can be formulated as

$$\begin{aligned} T &= m \left( r^2 (1 + \sin(\phi - \theta)) (\dot{\phi} - \dot{\theta})^2 \right. \\ &\quad \left. + rl (\cos \phi - \sin \theta) (\dot{\phi} \dot{\theta} - \dot{\theta}^2) + \frac{1}{2} l^2 \dot{\theta}^2 \right), \\ V &= \frac{1}{2} k_t (\phi_0 - \phi)^2 \\ &\quad + mg (r + r \sin(\phi - \theta) + l \sin \theta). \end{aligned} \quad (9)$$

The latter includes gravitational and elastic potential energies. The symbol  $g$  represents the gravity constant. Assuming motion of the R-SLIP model in the stance phase is pure rolling without sliding, the ground reacting force does not contribute. Therefore, the system is energy conservative and the following equations hold:

$$\begin{aligned} \frac{d}{dt} \left( \frac{\partial T}{\partial \dot{\theta}} \right) - \frac{\partial T}{\partial \theta} + \frac{\partial V}{\partial \theta} &= 0, \\ \frac{d}{dt} \left( \frac{\partial T}{\partial \dot{\phi}} \right) - \frac{\partial T}{\partial \phi} + \frac{\partial V}{\partial \phi} &= 0. \end{aligned} \quad (10)$$

By importing (9) into (10) and rearranging the equations, the double derivatives of the generalized coordinates,  $\ddot{\theta}$  and  $\ddot{\phi}$  can be expressed as nonlinear functions of other state variables  $\ddot{\theta} = A(\theta, \phi, \dot{\theta}, \dot{\phi})$ ,  $\ddot{\phi} = B(\theta, \phi, \dot{\theta}, \dot{\phi})$ . Therefore, the equations of motion of the R-SLIP model in its stance phase can be expressed in the state-space form

$$\frac{d}{dt} \begin{bmatrix} \theta \\ \phi \\ \dot{\theta} \\ \dot{\phi} \end{bmatrix} = \begin{bmatrix} \dot{\theta} \\ \dot{\phi} \\ A(\theta, \phi, \dot{\theta}, \dot{\phi}) \\ B(\theta, \phi, \dot{\theta}, \dot{\phi}) \end{bmatrix}. \quad (11)$$

The state of the mass can be derived by importing the solutions of (11) into (8) or its derivative. On the other hand, the motion of the R-SLIP model in its flight phase is ballistic and affected by gravity only, so the equations of motion of the

R-SLIP model can be described as

$$\begin{bmatrix} x_f \\ z_f \end{bmatrix} = \begin{bmatrix} x_{LO} + \dot{x}_{LO}t \\ z_{LO} + \dot{z}_{LO}t - \frac{1}{2}gt^2 \end{bmatrix}, \quad (12)$$

where the symbols f and LO indicate the flight phase and lift-off, respectively. Figures 3(e) and (f) show a typical trajectory and ground contact force of the R-SLIP model during locomotion.

## 4. Preparation for model performance analysis

### 4.1. Continuous running of the R-SLIP model

The R-SLIP model described in (11) and (12) is a conservative system. Thus, the system dynamics in a full stride, including both stance and flight phases, can be numerically evaluated with four preset system parameters ( $r$ ,  $k_t$ ,  $m$ ,  $l$ ) and chosen system initial conditions (ICs). The ICs of the model are usually given at the moment of touchdown (i.e., beginning of the stance phase), which includes landing angle ( $\beta$ ), touchdown speed ( $v$ ), and touchdown angle included by the touchdown velocity and horizontal line ( $\alpha$ ) as shown in figure 1(a). With these definitions, the ICs of state variables shown in (11) can be represented as

$$\begin{bmatrix} \theta_{td} \\ \phi_{td} \end{bmatrix} = \begin{bmatrix} \pi - \phi_0 - \beta \\ \phi_0 \end{bmatrix}$$

$$\begin{bmatrix} \dot{\theta}_{td} \\ \dot{\phi}_{td} \end{bmatrix} =$$

$$\begin{bmatrix} -r(1 + \sin(\phi_{td} - \theta_{td})) - l \sin(\theta_{td}) & r(1 + \sin(\phi_{td} - \theta_{td})) \\ -r \cos(\phi_{td} - \theta_{td}) + l \cos(\theta_{td}) & r \cos(\phi_{td} - \theta_{td}) \end{bmatrix}^{-1} \begin{bmatrix} \dot{x}_s \\ \dot{z}_s \end{bmatrix} \quad (13)$$

with

$$\begin{bmatrix} \dot{x}_s \\ \dot{z}_s \end{bmatrix} = v \begin{bmatrix} \cos \alpha \\ -\sin \alpha \end{bmatrix},$$

where subscript td indicates the moment of touchdown. Note that the torsion spring is in its natural configuration at the moment of touchdown.

If the R-SLIP model runs properly in stance phase, at a certain moment it will initiate its flight phase. If its vertical velocity and acceleration meet the criteria

$$\begin{aligned} \dot{z}_s &> 0 \\ \ddot{z}_s &= -g, \end{aligned} \quad (14)$$

the model lifts off. Note that this condition is also equivalent to the zero ground reaction force or the leg springing back to its natural length. In addition, two conditions should be satisfied for continuous running: (i) the horizontal velocity of the model at lift-off is forward

$$\dot{x}_{LO} > 0, \quad (15)$$

and (ii) height of the model at apex is large enough, so the follow-up touchdown with preset landing angle ( $\beta$ ) after

ballistic flight is feasible:

$$z_{LO} + \frac{\dot{z}_{LO}^2}{2g} > r + r \sin \beta. \quad (16)$$

In short, equations (14) to (16) are essential to grant the existence of the next stance phase. Since the energy of the model in flight phase is conservative and the landing angle ( $\beta$ ) is preset, the touchdown speed ( $v$ ) at every touchdown is the same. Moreover, touchdown angle of the model in its next stance phase can be defined as

$$\alpha = \arccos \left( \frac{\dot{x}_{LO}}{v} \right). \quad (17)$$

By importing these values into (13) and then into (11), dynamic behavior of the model in its next stance phase can be simulated. With the same iteration method, the continuous running behavior of the model from stride to stride can be derived.

The numerical simulation may fail when the R-SLIP configures in two extreme conditions as shown in figures 3(c), (d)—when the torsional spring contacts the ground as shown in figure 3(c), and when the mass, torsion spring, and contact point align in a line segment as shown in figure 3(d). In both cases the torque generated by the torsional spring cannot be balanced. In the follow-up steps-to-fall analysis, these two cases are regarded as the same as other falling down conditions.

### 4.2. Setup for comparison with the SLIP model

In addition to reporting the performance of the R-SLIP model, the SLIP model is also reported for better understanding of the characteristics and differences caused by the structure of rolling contact and torsional spring. Thus, the equivalent linear spring stiffness of the R-SLIP model needs to be defined, where the  $k_{10\%}$  rule utilized in [29] is adopted in the analysis. The  $k_{10\%}$  is the linear spring's stiffness at which the spring's length is compressed to 10%. Because the natural linear spring length of the model varies when the ground contact point changes, it is set equal to the diameter of the circular rim ( $l_0 = 2r$ ), at which the mass is located right above the ground contact point as shown in figure 4. The angle  $\phi_{10\%}$  of the R-SLIP model while its equivalent linear spring is compressed to 10% can be expressed as

$$\phi_{10\%} = \cos^{-1} \left( \frac{l^2 + l_a^2 - l_b^2}{2(l)(l_a)} \right) \quad (18)$$

with

$$l_a = \sqrt{l_0^2 - l^2} \text{ and } l_b = 0.9l_0.$$

The associated linear spring force  $F$  is

$$F_{10\%} = \frac{l_b k_t \left( \frac{\pi}{2} - \phi_{10\%} \right)}{(l)(l_a) \sin(\phi_{10\%})}. \quad (19)$$



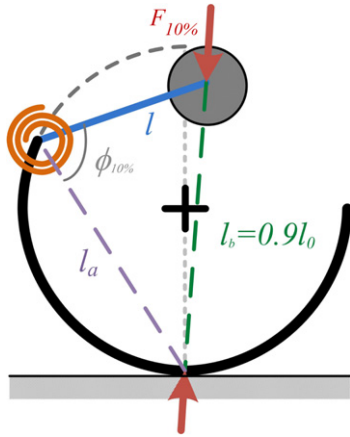


**Figure 4.** Configuration of the R-SLIP model where the equivalent linear spring stiffness  $k_{10\%}$  is defined.

Thus, and the equivalent linear spring stiffness  $k_{10\%}$  is

$$k_{10\%} = F_{10\%}/0.1l_0. \quad (20)$$

To make the touchdown conditions of both R-SLIP and SLIP models similar and comparable, in the following analysis their landing angles are set differently but with similar geometrical configurations as shown in figure 1. In this definition, the landing angle of the SLIP model ( $\beta_{\text{SLIP}}$ ) has a relationship to that of the R-SLIP model ( $\beta_{\text{RSLIP}}$ ) defined as  $\beta_{\text{SLIP}} = \pi/4 + \beta_{\text{RSLIP}}/2$ .

#### 4.3. Setup for dimensionless analysis

Dimensional analysis is adopted in the paper for generalized analysis. Because the model development is aimed for future robotic applications, the method of generating dimensionless analysis is based on the characteristics of the empirical robot systems. Among four system parameters and three ICs of the R-SLIP model, three system parameters ( $r, m, l$ ) are generally fixed in given empirical systems. In contrast, the last system parameter  $k_t$  can be utilized for system tuning, and three ICs ( $v, \alpha, \beta$ ) can be manipulated during locomotion. More specifically, the compliance  $k_t$  of the robot legs can be fabricated to a specifically designed value for stable running. The touchdown speed ( $v$ ) and touchdown angle ( $\alpha$ ) of the robot can be adjusted through leg control in the previous stance phase during running. The landing angle ( $\beta$ ) of the robot can be adjusted in the flight phase. Therefore, in the following analysis, the system parameters ( $r, m, l$ , i.e., robot mass and dimensions) are considered fixed, while the system parameter  $k_t$  and three ICs ( $v, \alpha, \beta$ ) are subjected to variance. The system parameters ( $m, r$ ) of the R-SLIP model and  $m, l_0$  of the SLIP model, as well as the standard gravity  $g$ , are utilized for generating dimensionless parameters, which include:

Dimensionless stiffness of the torsional spring  $\tilde{k}_t = k_t/(mgl_0)$ ,

Dimensionless stiffness of the linear spring  $\tilde{k} = kl_0/(mg)$ ,

Dimensionless landing angle  $\tilde{\beta} = \beta$ ,

Dimensionless touchdown speed  $\tilde{v} = v/\sqrt{gl_0}$ ,

Dimensionless touchdown angle  $\tilde{\alpha} = \alpha$ ,

Note that  $l_0 = 2r$  in the R-SLIP model.

## 5. Steps-to-fall performance of the R-SLIP model

Steps-to-fall is a quantitative index of the dynamic model, which reveals how many steps the model can perform dynamically (i.e., with stance and flight phases) without falling down. This index has been used in [29, 36, 37]. With a given set of ICs, if the model can run with more steps than the preset threshold, it is considered stable. The threshold is set to 24 strides, the same as that reported in the literature [36, 37]. Our initial investigation revealed that performance of the model with 24 strides as threshold is similar to that with 100 or more strides. Although stability of the model cannot be precisely judged by steps-to-fall analysis, this index does reveal the stability trend of the model, which helps with the follow-up return map analysis of detailed stability property and state transition from stride to stride. In addition, because graphic representation of the analysis is suitable for variations of two variables, the touchdown angle  $\tilde{\alpha}$  and landing angle  $\tilde{\beta}$  are chosen to be varied from  $0 \sim \pi/2$ , which covers all reasonable angles of these two variables. The other two out of four factors,  $\tilde{k}_{10\%}$  and  $\tilde{v}$ , are fixed in each plot, and their variations are plotted in different sub-figures next to each other.

Figure 5 plots steps-to-fall analysis of the SLIP model and the R-SLIP model with four given touchdown speeds and three different spring stiffnesses. The color bar at the bottom of the plot indicates the number of strides the system can perform before it falls. The results of steps-to-fall analysis reveal several facts. (i) For comparison of the subplots with different touchdown speeds (i.e., horizontal direction), the stable region increases if the touchdown speed increases. If the touchdown speed is too low, the stable region merely exists. Thus, when touchdown speed of the model with a given fixed stiffness increases, the model can stably run with a larger variation of landing angles. (ii) The suitable landing angle increases while the stiffness  $\tilde{k}$  (or  $\tilde{k}_{10\%}$ ) increases. The phenomenon is similar to the two-segment leg model reported in [29]. In contrast, the suitable landing angle decreases while the touchdown speed  $\tilde{v}$  increases. (iii) For each subplot, the suitable landing angle for stable running is limited to a small range. By comparison, the touchdown angle can tolerate a large variation. (iv) In the R-SLIP model, there appears a second cluster of the stable region in the high touchdown speed and low stiffness case, and this phenomenon will be discussed in section 6. (v) The stable region of the R-SLIP model is larger than that of the SLIP model under the same parameter settings. Thus, the R-SLIP model can tolerate a larger disturbance during running. In addition, owing to its rolling characteristics, the R-SLIP model with large touchdown angle has a stable running region, which is not observed in the SLIP model.

If the R-SLIP model can be regarded as the ‘template’, of the empirical legged robot [4], the trends and results of the model shown in steps-to-fall offer some positive lessons for

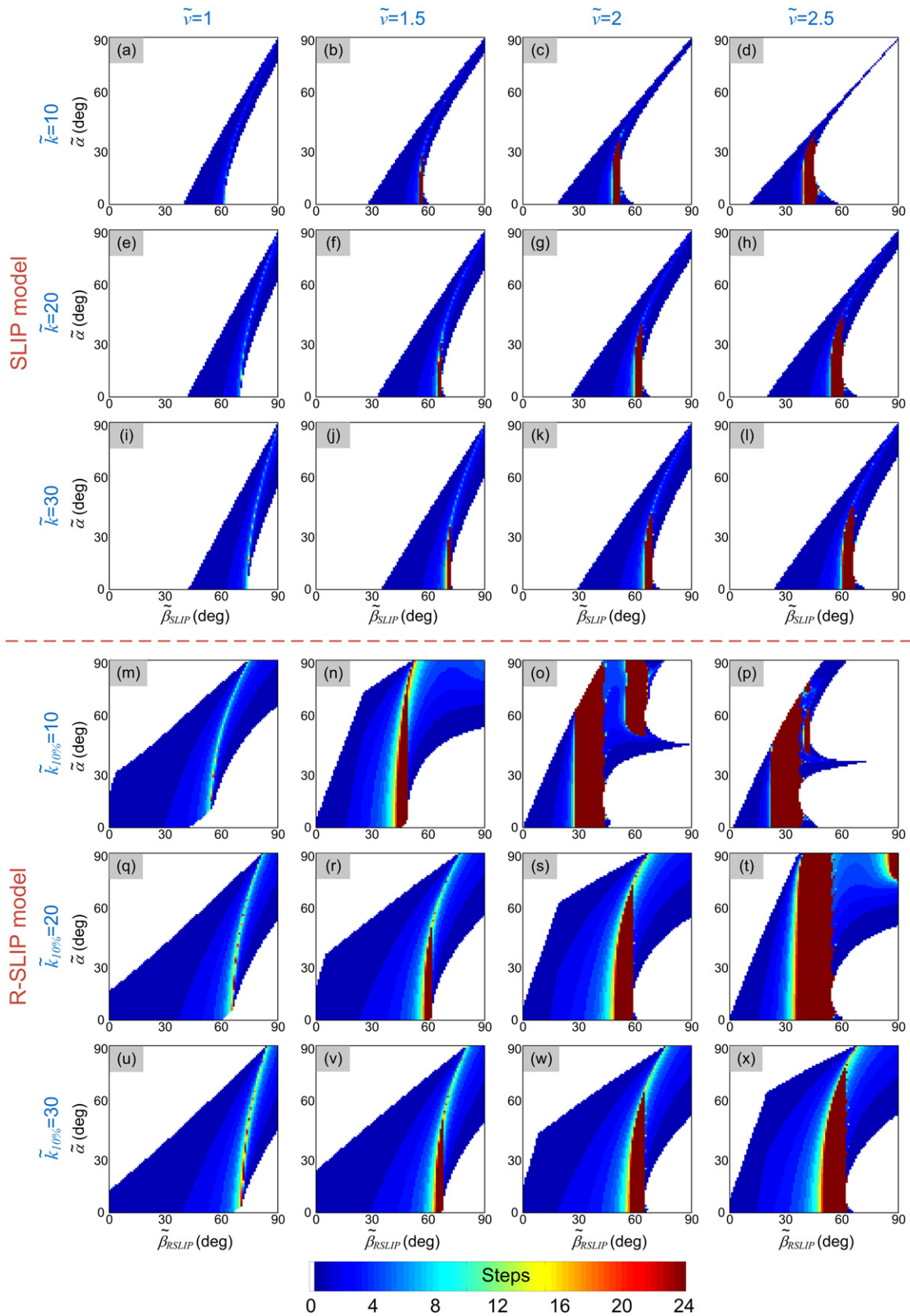


**Figure 5.** Steps-to-fall analysis of (a)–(l) the SLIP model and (m)–(x) the R-SLIP model with four touchdown speed  $\tilde{v} = 1, 1.5, 2$  and  $2.5$  and three spring stiffness ( $\tilde{k}$  or  $\tilde{k}_{10\%} = 10, 20,$  and  $30$ ). The regions with different colors indicate the number of consecutive steps the model can perform before it falls down. The color bar at the bottom shows the relation between the colors and the numbers of steps.

designing and controlling legged robot locomotion. The touchdown speed is directly linked to the energy of the robotic system, and it is hard to alter. In contrast, the landing angle and touchdown angle are easier to be disturbed in the empirical system. As a result, these two angles should be well controlled for stable locomotion. As shown in figure 5, the stable running of the robot with given leg stiffness and touchdown speed requires a very precise landing angle but much less constraint on the touchdown angle, no matter how stiff the leg is. This leads to the conclusion that, between these two angles, the landing angle is the main factor needing control. This is good news because the landing angle in general can be directly controlled by leg configuration (i.e., by joint motors). In contrast, the touchdown angle is mainly determined by the take-off and ballistic flight conditions, which are hard to control. The significance of choosing an adequate landing angle for the robot's cyclic motion is also mentioned in [6].

Furthermore, the results of steps-to-fall are in line with reported animal behaviors, which suggest that animals extend their stride length while increasing their running speed [38]. The steps-to-fall analysis shows that the model tends to decrease its landing angle while the touchdown speed increases for stable running. In fact, the outcome of lowering the landing angle is equal to increasing the stride length. This observation implies that the R-SLIP model can not only be utilized as a control guidance for a RHex-style robot with half-circular legs, but is also suitable for understanding animal behaviors.

## 6. Return map analysis of the R-SLIP model

In addition to the steps-to-fall analysis which provides rough trends of the model's stability, return map analysis was conducted to evaluate in detail the state transition from stride to stride and to search for fixed points. In this single-step analysis, the stability is judged by the relationship of a specific variable  $x$  between its current  $i$ th state and its next  $i + 1$ th state as

$$x_{i+1} = f(x_i, u_i), \tag{21}$$

with

$$\begin{aligned} x &= \alpha, \\ u &= \beta, \end{aligned}$$

where  $u$  is the control input of the system. The fixed point exists when the next state of this variable is the same as its current state

$$x^* = x_{i+1} = x_i. \tag{22}$$

The dimensionality of the model determines the method of performing return map analysis. The dimensionality of the R-SLIP model is similar to that of the SLIP model by merely having one more geometrical parameters. The R-SLIP needs two parameters ( $r, l$ ) to define the configuration, and the SLIP model only needs one ( $l_0$ ). The remaining two parameters ( $m, k$ ) and three ICs ( $v, \alpha, \beta$ ) are similar. In general the

variation of the variables ( $k, v, \alpha, \beta$ ) should be taken into account for return map analysis. However, as with the analysis process of the SLIP model, some assumptions and intrinsic properties help to reduce the complexity of the problem. The landing angle  $\beta$  is regarded as a 'control input' because it can be empirically controlled on the robot. Following this, the touchdown speed  $v$  is automatically fixed at the touchdown moment to conserve energy. In addition, it is also reasonable to freeze the stiffness of the torsion spring  $k$ , as is widely used on the SLIP. As a result, only the touchdown angle  $\alpha$  is an undetermined factor to be investigated, and the process is very similar to that of the SLIP model. Therefore, the analysis is regarded as a 1-dimensional problem. In this one-dimensional case, the eigenvalues of the Jacobian matrix within the unit disk is equal to the slope condition of the fixed points:

$$\left| \frac{dx_{i+1}}{dx_i} \right|_{x^*} < 1. \tag{23}$$

Among four variables ( $\tilde{k}_{10\%}, \tilde{v}, \tilde{\alpha}, \tilde{\beta}$ ), the touchdown angle  $\tilde{\alpha}$  is selected for return map analysis because, in the empirical system, this state is usually passively determined by other states and is hard to control. By investigating its return map, it can be revealed how stably the system runs. The range of the touchdown angle in the plot covers the whole adequate range  $0 \sim \pi/2$ , and the landing angle varies with  $\pi/36$  increment (i.e.,  $5^\circ$ ).

Figure 6 plots the return maps of both SLIP and R-SLIP models, and several observations can be addressed. (i) The analysis results of the return map match those of the steps-to-fall. Taking the SLIP model with  $\tilde{k} = 10$  and  $\tilde{v} = 2$  as an example (i.e., figures 5(c) and 6(b)), the steps-to-fall analysis indicates that the stable region exists when the landing angle  $\beta$  is around  $50^\circ$  and the touchdown angle  $\alpha$  is between  $0^\circ$  and  $30^\circ$ . Correspondingly, the return map analysis shows existence of a stable fixed point located at  $\alpha = 10^\circ$  and  $\beta = 50^\circ$ . (ii) Regarding the R-SLIP model, taking condition  $\tilde{k}_{10\%} = 20$  and  $\tilde{v} = 2$  as an example (i.e., figures 5(s) and 6(h)), if the model with a small touchdown angle (e.g.,  $10^\circ$ ) lands on the ground with an adequate landing angle (i.e. around  $\tilde{\beta} = 55^\circ$ ), its motion is stable owing to the existence of stable fixed points. If the model has a larger landing angle (e.g.,  $65^\circ$ ), the motion becomes unstable. In addition, figure 5(s) reveals that the model with different landing angles has a similar trend. For example, the model with a landing angle ( $\beta$ ) higher than  $50^\circ$  will gradually decrease its touchdown angle during running, and vice versa. The stable fixed point of the SLIP model exists only when the touchdown angle is small. In contrast, the R-SLIP model with both low and high touchdown angles can be stabilized. For example, several stable fixed points exist at a high touchdown angle as shown in figure 6(f), and this result matches that in the steps-to-fall analysis as shown in figure 5(o).

Figure 6 also reveals that the major difference between the SLIP model and the R-SLIP model lies in the layout of all curves. The curves of the R-SLIP model are more concentrated around the line  $x = y$ , and these curves have small

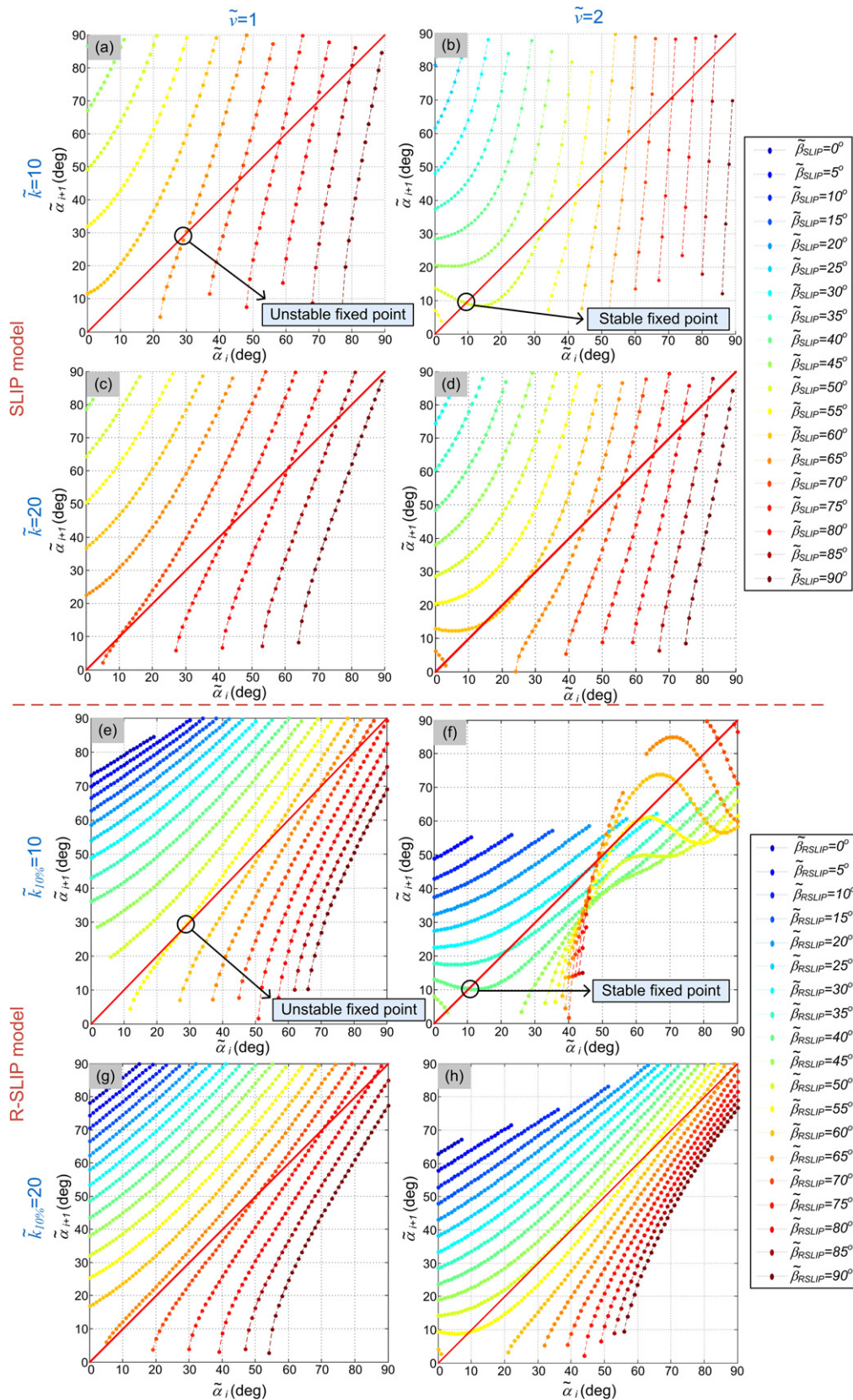


**Figure 6.** Return map of (a)–(d) the SLIP model and (e)–(h) the R-SLIP model with two touchdown speed ( $\tilde{v} = 1$  and  $2$ ) and two spring stiffness ( $\tilde{k}$  or  $\tilde{k}_{10\%} = 10$  and  $20$ ). Curves with different colors represent different landing angle  $\tilde{\beta}$ .

slopes. In contrast, those of the SLIP model are scattered. This observation implies that motion of the SLIP model is more sensitive because the touchdown angle may have a larger variation from stride to stride. This phenomenon suggests that the stable region of the R-SLIP model is larger than that of the SLIP model, consistent with the observation obtained in figure 5. In addition, figure 6 can also serve as the guideline for robot control when the robot runs with the R-SLIP/SLIP model as the template. By actively adjusting the landing angle in real time, motion of the robot can converge to the state where the stable fixed point is located.

It is important to understand the locations and trends of fixed points within the overall parameter space, especially when the analysis serves as the guideline for empirical robot control. Figure 7 plots distribution of the fixed points of the R-SLIP model and the SLIP model. Basically, the fixed points on the line  $y = x$  (i.e., the red straight line) shown in figure 6 form a curve in figure 7. Because there are four variables in the dimensionless analysis ( $\tilde{k}_{10\%}$ ,  $\tilde{v}$ ,  $\tilde{\alpha}$ ,  $\tilde{\beta}$ ), and each plot can only contain variations of three variables, variation of the fourth variable is presented in different subfigures. Note that, to simplify model comparison, the  $x$ -axis of sub-figures (a)–(c) are all converted into touchdown notation of the R-SLIP,  $\tilde{\beta}_{R-SLIP}$ , by the method described in section 4.2. The figure reveals several facts: (i) the stability property of the R-SLIP or SLIP model with low touchdown speed (i.e.  $\tilde{v} = 1.0$ ) is not promising. The R-SLIP model has few stable fixed points when the stiffness is low, and the SLIP model has no stable point. Low touchdown speed implies low system energy. In this case, when the leg stiffness is comparably high, the model cannot keep moving forward because the leg spring compresses and decompresses too fast, which stops the mass from moving forward and pushes it backward. (ii) When the model's energy level gets higher (i.e.  $\tilde{v} = 2.0$  or  $3.0$ ), both models appear to have more stable fixed points. Though distribution of the stable fixed points of the R-SLIP model appears more irregular than that of the SLIP model, the R-SLIP model has stable fixed points with all ranges of stiffness. In contrast, the SLIP model has no stable fixed point in the case of  $\tilde{v} = 2.0$  and  $\tilde{k} = 5$  and of  $\tilde{v} = 3.0$  and  $\tilde{k} = 5, 10$ . Thus, with a given energy level of the model, the R-SLIP model can tolerate a wider range of stiffness. (iii) Considering the SLIP model with a specific stiffness, when the touchdown speed increases, the fixed points in the figure move left, which indicates that the associated landing angle decreases. In contrast, the associated touchdown angle remains similar. As for the R-SLIP case, when the touchdown speed increases, the change of fixed point distribution of the R-SLIP model is irregular. One clear observation is that the stable fixed point exists at a wide range of touchdown angles. In addition to the original cluster of stable fixed points extending its associated touchdown angles, another cluster of stable fixed points appears with high values of touchdown angles. For example, when  $\tilde{k}_{10\%} = 20$  and  $\tilde{v} = 3.0$ , the R-SLIP model has one cluster of stable fixed points where the touchdown angle ranges from  $5^\circ$  to  $56^\circ$ , and another cluster where the touchdown angle ranges from  $60^\circ$  to  $78^\circ$ . This observation implies that the R-SLIP model can generate not only running but also

hopping motion as the sketches show in figure 7(f). The dynamic motion of the R-SLIP model seems to have a wider variation than that of the SLIP model. (iv) No fixed point exists when the models have high landing angles and low touchdown angles (i.e., lower right corner of the figures). In this case, the models pose vertically but the touchdown velocity lies horizontally, where the spring can barely be compressed, so the model falls. (v) The R-SLIP model has scattered stable fixed points at very high landing and touchdown angles, which is not observed in the SLIP model. The motion sequence of the R-SLIP model in this condition is plotted in figure 8. After the model touches down, it rolls back when the torsional spring compresses. Thus, though the mass keeps moving forward, the ground contact point actually moves backward. With the right momentum of the mass which pulls the leg rolling forward, the follow-up motion of the model is similar to other ordinary cases. In contrast to the SLIP model which contacts the ground at a specific point for each stance phase, the R-SLIP model has rolling contact. In normal cases the ground contact point of the model in stance phase moves forward. Though the motion shown in figure 8 is unusual, it does demonstrate a special characteristic owing to the unique rolling contact of the R-SLIP model.

Distribution of the fixed points shown in figure 7 reveals that change of the stiffness on model stability is similar to change of touchdown speed. The effect of increasing the touchdown speed is at some level equivalent to decreasing the spring stiffness. The touchdown speed represents the amount of kinetic energy preserved in the system. In contrast, the spring stiffness represents how much and how quickly the energy can be stored as the spring potential. Thus, for a system with a given mass, one would expect these two factors to match each other in a certain range for stable and continuous running. To further investigate the relation between these two factors, we have computed the number of stable fixed points in each parameter setting ( $\tilde{k}$ ,  $\tilde{v}$ ) within a wide range of the above parameters and present the results in figure 9. Note that numbers of stable fixed points is also determined by the precision of numerical computation; in this plot  $2^\circ$  is utilized. In this demonstration the absolute value of the numbers is not the main concern, but the relative value is. Several observations can be made: (i) there exists a lower limit of touchdown speed of the model for stable running. (ii) When the system energy increases (i.e.,  $\tilde{v}$  increases), the stiffness range of the model for stable running increases, and the stiffness value also increases as expected. (iii) The stable region of the R-SLIP model is larger than that of the SLIP model.

The trends observed in figure 9 matches reported animal behavior, wherein leg stiffness increases when running faster [29, 39]. Thus, when animals want to run faster and keep locomotion stable without dramatic adjustment of body state, simultaneous adjustment of leg stiffness and landing angle is an effective strategy. In contrast, for those robots with pure passive compliant legs where stiffness is not adjustable, the robot can only stabilize its running locomotion by adjusting its landing angle. In that case, the achievable range of stable

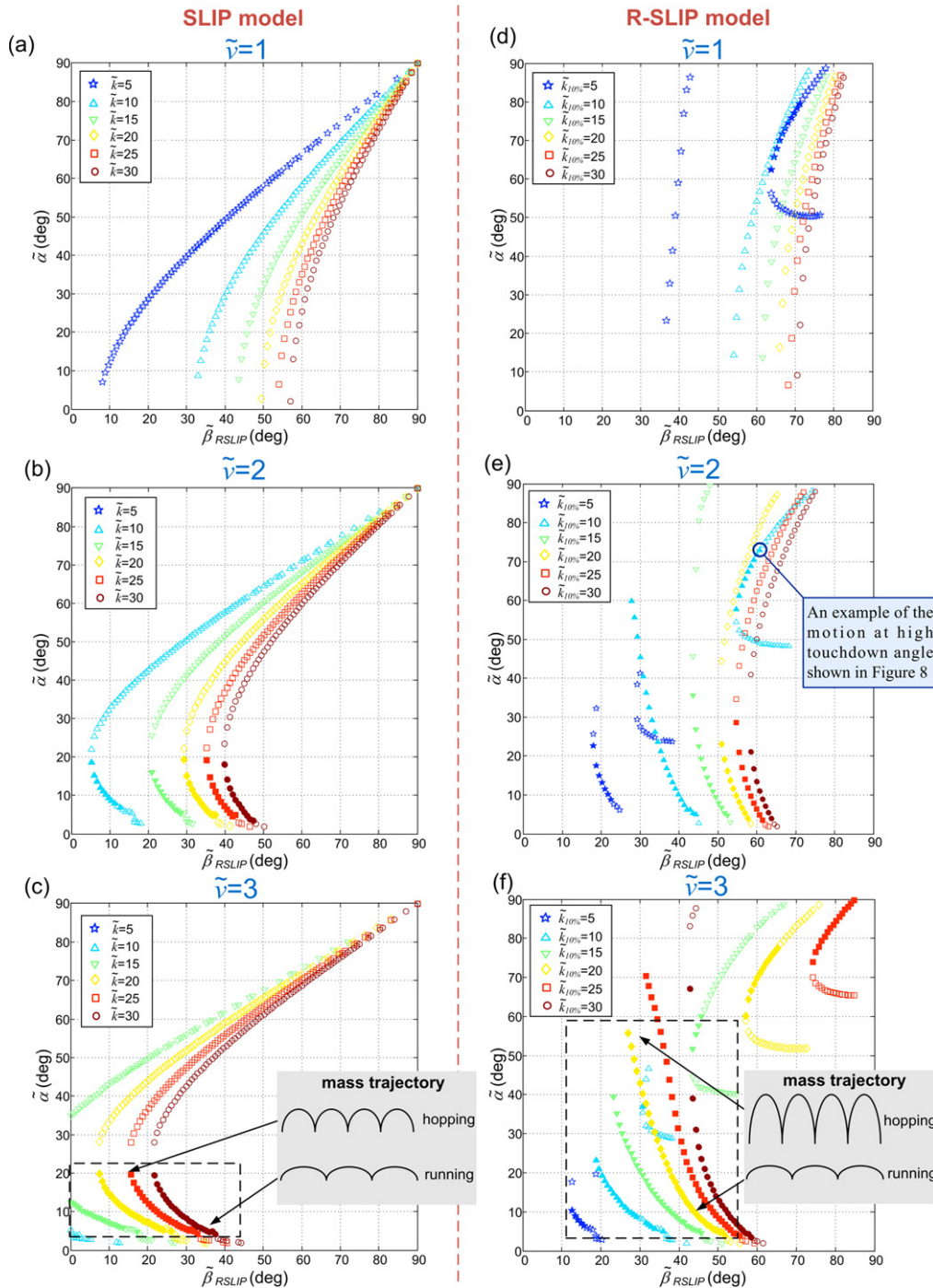


**Figure 7.** The fixed points of the SLIP model (a)–(c) and the R-SLIP model (d)–(f) with various parameter settings. The dimensionless touchdown speeds are 1.0 in (a), 2.0 in (b), and 3.0 in (c), respectively. The dimensionless stiffness ranges from 5 to 30, shown in different styles and colors of markers. Solid and hollow markers represent stable and unstable fixed points, respectively.

running will be limited, so selection of nominal stiffness is important.

Figure 9 can also be utilized for finding the dynamic locomotion region of the robot. The robot’s forward velocity is usually preset and limited by the power of the actuator, so the corresponding range of landing speed  $v$  can be roughly estimated. According to the analysis results, the suitable stiffness of the robot can be chosen based on the information provided in figure 9. For example, if the desired running

speed of the robot with a half-circular leg is about  $\tilde{v} = 3$ , the adequate stiffness for creating stable manner is around  $\tilde{k}_{10\%} = 20$ .

The return map analysis of the R-SLIP model confirms that the model has ‘self-stable’ gaits, just like the SLIP model [40]. With adequate ICs ( $v, \alpha, \beta$ ), and system parameters ( $r, k_t, m, l$ ), the model can stably run at or around the fixed point without control effort. Thus, if the robot can be operated to run like the R-SLIP model within its self-stable region, the

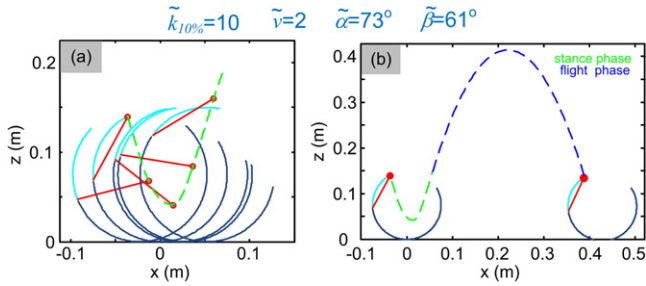


**Figure 8.** (a) The motion sequence in stance phase of the R-SLIP model with high touchdown speed and large touchdown angle. (b) The mass trajectory of the resulting hopping motion.

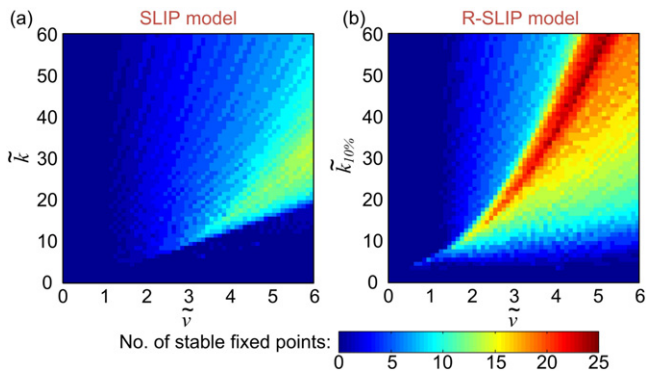


**Figure 9.** Numbers of stable fixed points of the R-SLIP model (a) and the SLIP model (b) within a range of touchdown speeds and stiffness.

power imported to the robot would only be used to overcome mechanical loss and disturbance from the environment. The robot should run very efficiently. Figure 7 also reveals that the usable ranges of landing angle and touchdown angle for stable running are wide, especially for the model with larger touchdown speed. Taking  $\tilde{v} = 3$  and  $\tilde{k}_{10\%} = 25$  as an example (i.e. orange squared markers in plot (f)), the stable range of the touchdown angle of the R-SLIP model can be nearly as wide as  $85^\circ$ . Under the same conditions, the SLIP model can allow only a  $15^\circ$  variation of its touchdown angle for stable running. In addition, because the touchdown angle is generally determined by take-off and ballistic conditions of the model, it is very easy to be disturbed. A wide allowable touchdown angle for stable running is truly an advantage.

## 7. Using the R-SLIP model as the template for a RHex-style robot for dynamic running

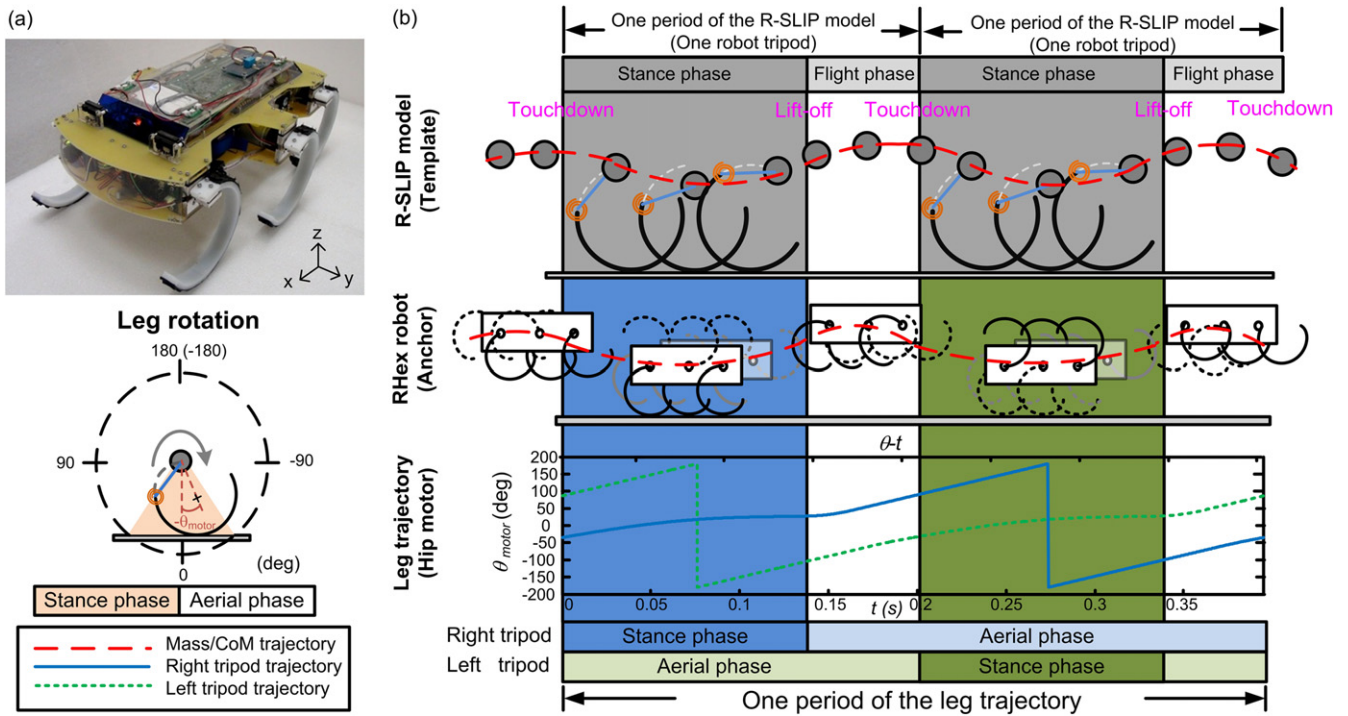
The promising intrinsic stability of the R-SLIP model suggests that it may be a good template [4] for dynamic running on a multi-legged robot. Because the planar R-SLIP model contains only a point mass, it is often used to represent the center of mass (CoM) motion of the robot in the sagittal plane. This setting defines how the original complex platform (i.e., the ‘anchor’) collapses to the low-DOF R-SLIP model (i.e., the ‘template’). With this definition, the remaining DOFs

of the platform should be maintained at stable values or no effect on motion of the R-SLIP model, including the lateral motion and orientation of the platform. If the above criteria are held, then the platform should ideally behave like the R-SLIP model. Through experimental investigation, we have found that the empirical robot implemented with this strategy can indeed directly excite its dynamic running behavior (i.e., with flight phase) without any parameter tuning or trajectory modification. The details will be described in the following paragraphs.

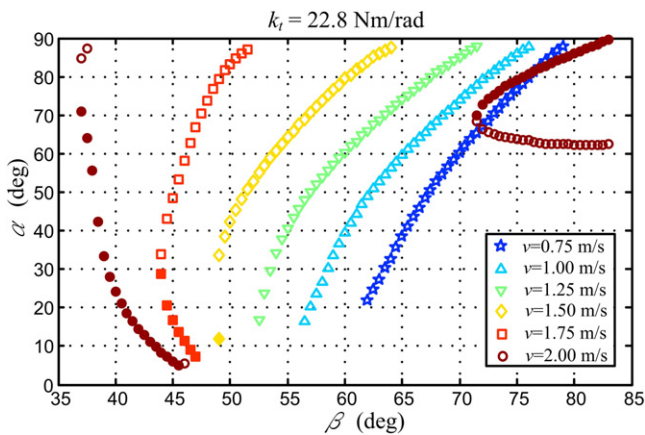
The RHex-style robot shown in figure 10(a) is utilized for the above ‘template and anchor’ experimental evaluation. RHex originated from the University of Michigan [13]. It is a hexapod robot with only one active rotational DOF per leg, with each leg made with compliant materials, mimicking the elastic behavior of running animals [1]. The robot utilized here is a reproduced version of RHex, with similar morphology but different size, weight, mechatronic setup, and control architecture. Detailed specifications can be found in [41]. While designing the robot, the leg stiffness is approximately selected based on the mouse-to-elephant curve [42] and the natural frequency of the one-dimensional hopper, where [43] has more details. The widely-used alternating tripod gait is adopted as the fundamental robot gait for these running experiments owing to its advantages of stable and fast locomotion. The legs in a tripod provide stable motion of the spatial rigid robot body (i.e., less pitch and roll). In addition, the two tripods are programmed to move in an alternating and symmetric manner; thus the robot should ideally move straight ahead (i.e., with less lateral displacement and yaw motion). As a result, motion of the four un-modeled DOFs of the real robot should have minimum variations.

Figure 10(b) shows the schematic motion sequence of the robot with a tripod gait and the R-SLIP model, the motion mapping between the ‘template and anchor’. Because the robot is set to move like the R-SLIP model, a full stride should include a stance phase and flight phase. In order to let the CoM move like the R-SLIP model in the stance phase, three legs of the tripod are synchronically actuated and rotated according to the R-SLIP trajectory while they roll on the ground. Based on the assumption that the robot body remains horizontal during the whole stance phase, the leg orientation with respect to the body is actually equal to the generalized coordinate  $\theta$  of the R-SLIP model as shown in figure 10(b). On the other hand, the period of the leg in its flight phase takes much longer than that of the R-SLIP model because the two tripod legs are alternating. The flight phase of the leg covers two flight phases and one stance phase of the R-SLIP model as shown in figure 10(b).

The quantitative model-robot mapping and the motion design procedure is described as follows. The mass  $m$  and leg radius  $r$  of the model are based on the measurements of the empirical robot. The torsional stiffness  $k_t$  and the link length  $l$  of the model are simultaneously computed by the least squared errors of the measured force-deflection relations of the robot leg at various contact positions. The detailed process can be found in [43]. As a result, the four intrinsic parameters of the R-SLIP model ( $r, m, l, k_t$ ) can be yielded. Note that



**Figure 10.** Setup for ‘template and anchor’ experiments: (a) the RHex-style robot for experiments; (b) schematic motion sequence of the robot with a tripod gait and the corresponding motion of the R-SLIP model.



**Figure 11.** Fixed points distribution of the R-SLIP model with parameter settings matching the empirical robot.

**Table 3.** Parameters for running experiments.

<i>Robot specifications</i>		
Body mass	M	6.884 kg
Body length	L	0.47 m
Body width	W	0.23 m
Body height	H	0.17 m
Leg radius	R	0.075 m
<i>R-SLIP model parameters</i>		
Mass	$m$	6.884 kg
Leg radius	$r$	0.075 m
Rigid bar length	$l$	0.082 m
Torsion spring stiffness	$k_t$	22.8 Nm rad <sup>-1</sup>
Dimensionless torsional spring constant	$\tilde{k}_t$	2.25
Equivalent linear spring stiffness	$k_{10\%}$	4276.6 N m <sup>-1</sup>
Dimensionless equivalent linear spring stiffness	$\tilde{k}_{10\%}$	9.50

the model stiffness is set to three times the robot leg stiffness, to calibrate the single leg and the tripod locomotion of the model and robot. Table 3 lists the key parameters for analysis. Next, the three ICs should be selected. Among these, the touchdown speed is first to be designated because it strongly relates to the energy level of the robot. The empirical actuation device of the robot should be strong enough to provide enough leg actuation power to achieve the desired speed. Empirical investigation shows that the robot can run from 1 m s<sup>-1</sup> to 2 m s<sup>-1</sup>. Thus, speeds within this range and with an increment of 0.25 m s<sup>-1</sup> are chosen for experiments. Finally, the touchdown angle and landing angle are selected based on the results of stability analysis described on sections 5 and 6.

Figure 11 shows distribution of the fixed points where the parameters are matched to the robot specifications. This figure reveals that no stable fixed point exists while the robot runs with a touchdown speed of 1 m s<sup>-1</sup> or 1.25 m s<sup>-1</sup>. When the speed equals or exceeds 1.5 m s<sup>-1</sup>, the stable fixed points appear. For the low-speed case, because unstable fixed points appear with the touchdown angle  $\alpha = 15^\circ - 90^\circ$ , so  $\alpha = 20^\circ$  is selected. For the medium- to high-speed case, the smaller touchdown angle  $\alpha = 10^\circ$  is selected for less variation on vertical displacement. Thus, with selected  $v$  and  $\alpha$ , the landing angle  $\beta$  can be selected. With defined intrinsic parameters



and selected ICs, the complete trajectory of the R-SLIP model can be numerically computed, including the states of both stance phase and ballistic flight phase. Trajectory of the model in the stance phase is directly coded for leg actuation. Time durations of both phases of the model are used to compute the flight-phase time of the leg. With a complete leg trajectory programmed, the robot is now ready for ‘template and anchor’ experimental evaluation.

Experiments were executed with the ground truth measurement system (GTMS) to yield true body state. The GTMS is composed of two 500 Hz high-speed cameras (A504k, Basler) and two 6-axis force plates (FP4060-07, Bertec). The high-speed cameras were mounted on the top right and left sides of the runway. When a bright marker was placed within the runway, its spatial coordinate could be reconstructed from two simultaneously-captured images from two cameras. By installing three bright LEDs on top of the robot, the spatial 6-DOF body state could be derived according to the geometrical relations between the markers and the robot’s CoM. Six-axis force plates were placed in the middle of the runway to capture the force interaction between the robot and the ground. A detailed description of the GTMS can be found in [41].

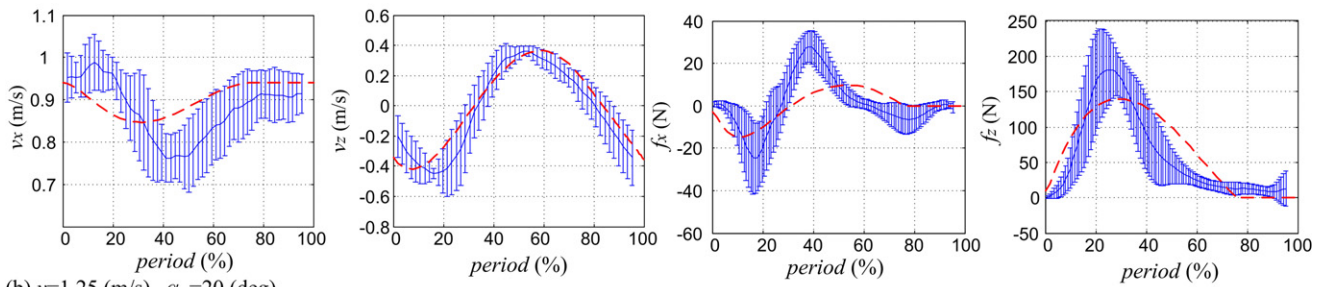
Figure 12 shows the velocity and ground reaction force of the robot versus time. The videos of the robot running with these conditions are included in the supplementary materials. The horizontal axis is normalized to one period of the R-SLIP model, and the actual periods are 0.223 s, 0.225 s, 0.183 s, 0.180 s, and 0.174 s, respectively. The figure reveals that the vertical velocities of the robot match those of the R-SLIP model quite well in all touchdown speeds. In contrast, the forward velocities of the robot only match the model when the touchdown speeds are low. When the speed increases, the velocity profiles remain similar but the achieved speeds seem lower than those of the model (about  $0.1 \text{ m s}^{-1}$  less). This discrepancy primarily results from ground slippage, which diverges the empirical behavior away from the model which assumes pure rolling contact. The force profiles of the robot and the model exhibit some discrepancy, but the trends remain similar to each other. We suspect this is mainly owing to the complex dynamics of the half-circular leg which is not able to be revealed in the reduced-order R-SLIP model. More specifically, the shape deformation of the R-SLIP model may catch the actual deformation pattern of the half-circular leg, which makes the velocity profiles resemble each other. However, during deformation the compliance effect of the leg and the model may not be the same; thus the force profiles appear with some magnitude of difference. Nevertheless the force profiles clearly show that the robot performs dynamic running behavior, where the vertical force profile has a single compression and the forward force profile has a brake-then-accelerate pattern, similar to the reduced-order spring-mass models such as the SLIP or R-SLIP model. In addition, the robot motion also exhibits an obvious flight phase, revealed in the portion with zero vertical ground reaction force. In sum, the robot can initiate its dynamic running behavior with the profiles based on the R-SLIP model.

Table 4 gives a statistical summary of the robot pitch and roll. The results are averaged from all experimental runs. Note that, even though the robot ran with pre-defined R-SLIP-based trajectories with no pitch or roll control strategy, the means of both pitch and roll were all less than  $0.6^\circ$  with stds less than  $2.2^\circ$ . Thus, the tripod locomotion formed by three compliant legs has a certain internal stabilization mechanism which keeps the body orientation changes small. This observation also confirms that the tripod approximated by a single ‘virtual leg’ utilized in this paper can be held. If the mean is not close to zero or the std is large, three legs of the same tripod may move according to different trajectories. In addition, pitch stds of the robot with  $\alpha = 10^\circ$  are in general smaller than those with  $\alpha = 20^\circ$ . The robot with the smaller touchdown angle during running has less leg compression, and the torque generated from unbalanced empirical leg compression is less, so the pitch variation of the robot during running can be maintained in a smaller range.

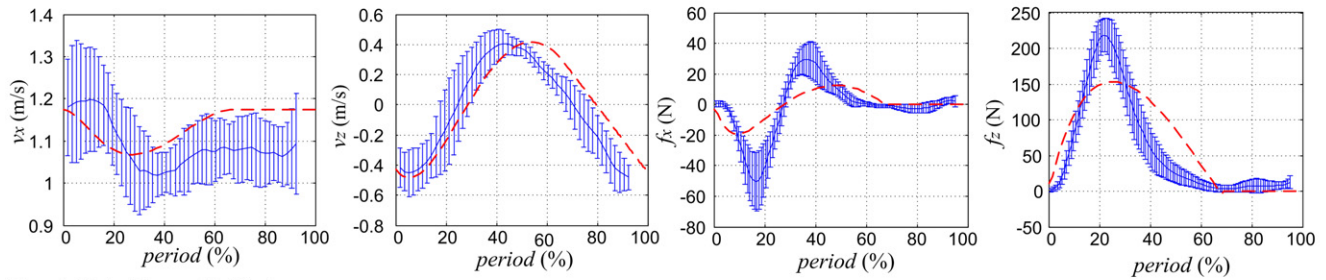
The behavior of the robot implemented with the SLIP model as the template was also evaluated. The fixed points of the SLIP model were searched for, and then the stable trajectories with conditions similar to those shown in figure 12 were implemented on the robot for experimental evaluation. The videos of the robot running with these conditions are included as supplementary materials. The videos clearly show that the robot implemented with SLIP trajectories performs walking locomotion (i.e., no moment where all legs are in the air) but cannot initiate running behavior as the SLIP model does. The robot also exhibits considerable pitch variation. In contrast, the robot implemented with R-SLIP trajectories indeed performs running behavior, for all experiments with different forward speed settings. The means and standard deviations of the ratios of the flight phase time to one period of the R-SLIP model and the robot are 0.235(0.066) and 0.242(0.073), respectively, and the results are quite similar to each other. The main reason for the SLIP’s failure results from the discrepancy of the leg driving pattern as shown in figure 13. The figure reveals that the robot implemented with the R-SLIP trajectories has a monotonic decreasing motor speed during stance phase, but that with SLIP trajectories has a speed close to constant, similar to the Buehler Clock setting [14]. This discrepancy yields incorrect leg spring compression/decompression patterns of the robot for dynamic motion.

The experimental results reported in this section reveal that, through correct mapping between ‘template and anchor’, dynamic behavior of the original complex system can indeed be initiated via the reduced-order model. Here, though the R-SLIP model may not perfectly capture the dynamics of the empirical, complex, and multi-legged robot, the strong resemblance between them offers the possibility of using the former to excite the dynamics of the latter. Without any parameter tuning, the parameters which make the R-SLIP model run also make the robot run, not only for one specific parameter set but for all five different sets. We believe this achievement is significant, since, in the past development of RHex, the initiation of its dynamics was not trivial. The

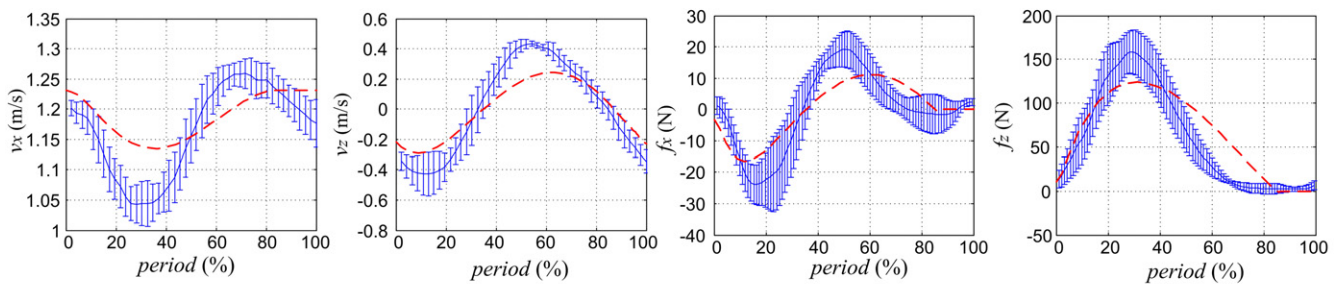
(a)  $v=1$  (m/s),  $\alpha =20$  (deg)



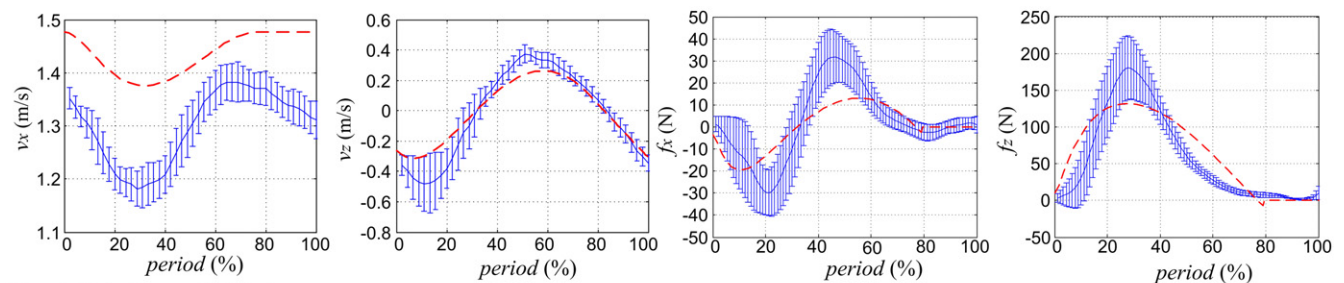
(b)  $v=1.25$  (m/s),  $\alpha =20$  (deg)



(c)  $v=1.25$  (m/s),  $\alpha =10$  (deg)



(d)  $v=1.5$  (m/s),  $\alpha =10$  (deg)



(e)  $v=1.75$  (m/s),  $\alpha =10$  (deg)

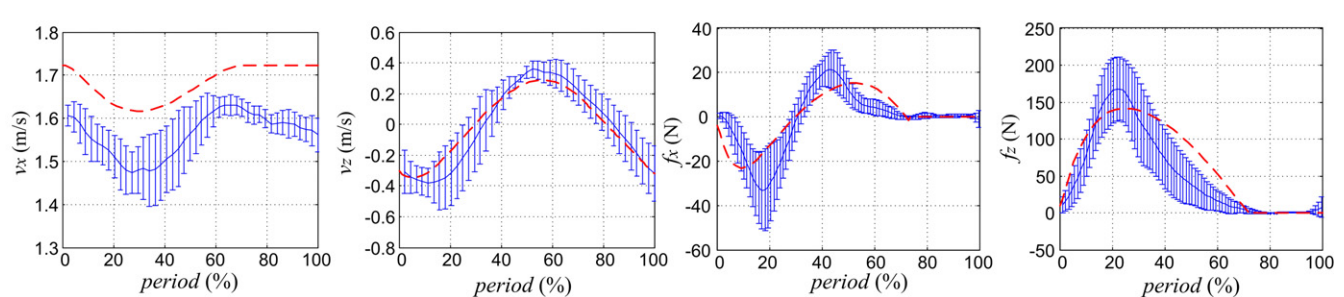


**Figure 12.** Velocity and ground reaction force of the robot (means, middle blue curves; top and bottom bars, standard deviations) and the R-SLIP model (red dashed curves) versus time. The symbols ( $v_x, v_z, f_x, f_z$ ) denote forward velocity, vertical velocity, forward ground reaction force, and vertical ground reaction force, respectively. The horizontal axis is normalized to one period of the R-SLIP model.

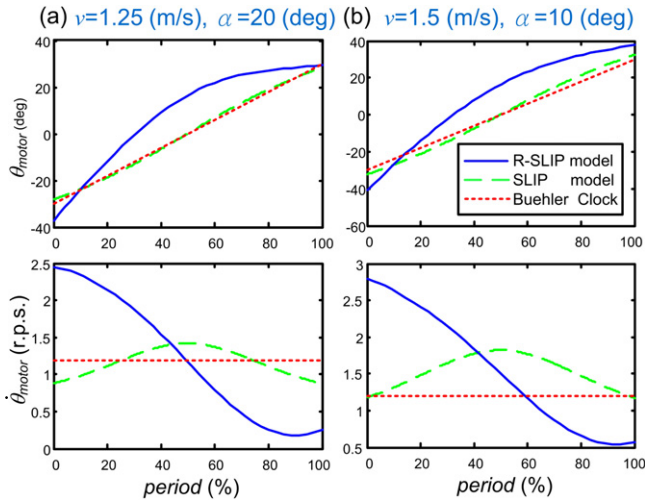


**Figure 13.** Stance-phase leg driving profiles of the robot implemented with the R-SLIP model, SLIP model, and the Buehler Clock. (a) and (b) plot different running conditions. The actual periods of the SLIP model and R-SLIP model in (a) and (b) are 0.134, 0.154, 0.116, and 0.142 s, respectively.

**Table 4.** Statistical summary of robot pitch and roll in experiments.

Initial conditions		Roll (°)		Pitch (°)	
$v$ (m s <sup>-1</sup> )	$\alpha$ (°)	Mean	std	Mean	std
1.00	20	-0.13	1.99	0.02	1.39
1.25	20	0.17	1.99	-0.13	1.96
1.25	10	-0.43	2.12	0.59	1.09
1.50	10	-0.36	1.78	0.20	1.07
1.75	10	-0.58	1.74	0.29	1.23

parameterized Buehler Clock is very useful in developing various walking gaits for rough terrain negotiation [14]. At that time, without carefully investigating the ‘template’ of RHex, initiation of its dynamic behavior was done through the optimization procedure. By setting energy-efficiency as the cost function, the robot after optimization performs a stable jogging gait. This is quite interesting, but provides limited insight in how to initiate running in continuous variation (i.e., with varying speeds or profile appearance). The approach reported in this paper provides the methodology of using merely a 2-DOF system as the ‘template’ to guide the dynamic behavior of the complex hexapod robot. Ideally, if the leg is precisely built according to the leg morphology of the R-SLIP model, the similarity in dynamic performance between the model and the robot may be higher. However, empirically it is still very challenging to build a lumped linear spring leg or torsional spring leg with extremely light weight. Thus, though the mapping of the half-circular leg of the robot to the R-SLIP leg may not be perfect, its light weight helps to keep motion similarity to a certain level. In short, the methodology and results reported here serve as the first and feasible important steps in developing the template-based dynamic behavior on the empirical robots.

## 8. Conclusion

We report on the development of the spring loaded inverted pendulum model with rolling contact (i.e., R-SLIP). On the analytical side, we would like to construct a simple model with rolling contact. By comparing its performance to the well-known SLIP model with similar simple morphology, we can understand how rolling affects the dynamic locomotion of the model. On the practical side, we would like to utilize the R-SLIP model as the reduced-order model of the compliant circular-shape material because the former is inspired by the linear elasticity model of the latter. Furthermore, from defining detailed mapping between the R-SLIP model and the empirical RHex-style robot with half-circular legs, the concept of ‘template and anchor’ can be experimentally evaluated.

The developed planar R-SLIP model has four intrinsic parameters. Compared to the SLIP model, one extra geometric parameter is introduced to compensate for the change of linear spring to torsional spring. Unlike the SLIP model that has point contact with the ground, the circular lower segment of the R-SLIP model exhibits rolling behavior to the ground. The quantitative formulation of the R-SLIP model was derived from the Lagrangian method, and steps-to-fall and return map were utilized for model behavior and stability analysis. The former examines whether the model with a specific set of parameters and ICs can successfully perform stable running for a specific number of strides without falling down. In contrast, the latter method provides a single step and one-dimensional analysis of the model from stride to stride. In addition, in order to perform a quantitative comparison to the SLIP model, the  $k_{10\%}$  method and dimensionless analysis were utilized.

The stability analysis of the R-SLIP model reveals several facts. First, as with the SLIP model, the R-SLIP model has self-stable gaits (i.e., with stable fixed points), and the stable region of the latter model is in general larger than that of the former. As the stiffness or touchdown speed of the model increases, the stable region of the model increases accordingly (i.e., the range of adequate landing angle for stable locomotion increases). Also, for a model of given stiffness and touchdown velocity to have stable locomotion, the touchdown angle can be varied within a wide range; in contrast, only a narrow range of landing angles can be selected. This phenomenon is actually good for empirical robot implementation because the landing angle can usually be directly controlled by leg configuration. In contrast, the touchdown angle is hard to control because it is mainly determined by the take-off and ballistic flight conditions. In addition, for the R-SLIP model with parameters in a certain range, the stable fixed points seem to be distributed in two clusters—one for regular running and the other for one-dimensional hopping, which is not observed in the SLIP model.

The R-SLIP model was embedded as the reduced-order ‘template’ in a more complex ‘anchor’, the RHex-style robot, via a simple open-loop control strategy and some mapping definitions. We chose several parameters and ICs sets of the R-SLIP model with stable running, and then directly deployed

these settings as the actuation commands of the empirical robot. By comparing motion of the R-SLIP model and the robot as well as the forward and vertical ground reaction forces, the trends of both trajectories match quite well. The robot can easily initiate its dynamic behaviors with flight phase with several different touchdown speeds without too much control effort. In addition, the close-to-zero means (less than  $0.6^\circ$ ) and small standard deviations of robot body pitch and roll (less than  $2.2^\circ$ ) during locomotion indicate that the extra DOFs of the empirical robot outside the R-SLIP model's DOFs maintain the stable value as assumed. Thus, the R-SLIP model can indeed serve as the template for the robot for dynamic locomotion. In contrast, the robot implemented with SLIP trajectories cannot initiate dynamic running behavior, and this further confirms that the template should be designed based on the robot's natural dynamics.

We are currently investigating the template-based closed-loop control strategy, so that the robot will be able to perform dynamic locomotion as well as behavior transition in a wider range of parameter settings. Also under investigation is the underlying mechanism whereby the robot's leg trajectory fails to match its natural dynamics, to the detriment of overall performance.

## Acknowledgment

This work is supported by the National Science Council (NSC), Taiwan, under contract NSC 100-2628-E-002 -021-MY3 and National Taiwan University, Taiwan, under contract NTU-CDP-102R7817.

## References

- [1] Alexander R M 1988 *Elastic Mechanisms in Animal Movement* (Cambridge: Cambridge University Press)
- [2] Blickhan R 1989 The spring mass model for running and hopping *J. Biomech.* **22** 1217–27
- [3] Holmes P *et al* 2006 The dynamics of legged locomotion: models, analyses, and challenges *SIAM. Rev.* **48** 207–304
- [4] Full R J and Koditschek D E 1999 Templates and anchors: neuromechanical hypotheses of legged locomotion on land *J. Exp. Biol.* **202** 3325–32
- [5] Raibert M 2000 *Legged Robots that Balance* (Cambridge, MA: MIT Press)
- [6] Poulakakis I, Smith J A and Buehler M 2005 Modeling and experiments of untethered quadrupedal running with a bounding gait: the scout II robot *Int. J. Robot. Res.* **24** 239–56
- [7] Poulakakis I, Papadopoulos E and Buehler M 2006 On the stability of the passive dynamics of quadrupedal running with a bounding gait *Int. J. Robot. Res.* **25** 669–87
- [8] Kimura H, Fukuoka Y and Cohen A H 2007 Adaptive dynamic walking of a quadruped robot on natural ground based on biological concepts *Int. J. Robot. Res.* **26** 475–90
- [9] Fukuoka Y, Kimura H and Cohen A H 2003 Adaptive dynamic walking of a quadruped robot on irregular terrain based on biological concepts *Int. J. Robot. Res.* **22** 187–202
- [10] Cham J G *et al* 2002 Fast and robust: hexapedal robots via shape deposition manufacturing *Int. J. Robot. Res.* **21** 869–82
- [11] Cham J G, Karpick J K and Cutkosky M R 2004 Stride period adaptation of a biomimetic running hexapod *Int. J. Robot. Res.* **23** 141–53
- [12] Kim S, Clark J E and Cutkosky M R 2006 iSprawl: design and tuning for high-speed autonomous open-loop running *Int. J. Robot. Res.* **25** 903–12
- [13] Altendorfer R *et al* 2001 RHex: a biologically inspired hexapod runner *Auton. Robots* **11** 207–13
- [14] Saranli U, Buehler M and Koditschek D E 2001 RHex: a simple and highly mobile hexapod robot *Int. J. Robot. Res.* **20** 616–31
- [15] Lin P C, Komsuoglu H and Koditschek D E 2005 A leg configuration measurement system for full-body pose estimates in a hexapod robot *IEEE Trans. Robot.* **21** 411–22
- [16] Lin P C, Komsuoglu H and Koditschek D E 2006 Sensor data fusion for body state estimation in a hexapod robot with dynamical gaits *IEEE Trans. Robot.* **22** 932–43
- [17] Lynch G A *et al* 2012 A bioinspired dynamical vertical climbing robot *Int. J. Robot. Res.* **31** 974–96
- [18] Johnson A M and Koditschek D E 2013 Toward a vocabulary of legged leaping. *IEEE Int. Conf. on Robotics and Automation (ICRA)*
- [19] Poulakakis I and Grizzle J W 2009 The spring loaded inverted pendulum as the hybrid zero dynamics of an asymmetric hopper *IEEE Trans. Autom. Control* **54** 1779–93
- [20] Ankarali M M and Saranli U 2011 Control of underactuated planar pronking through an embedded spring-mass hopper template *Auton. Robots* **30** 217–31
- [21] Koepl D and Hurst J 2011 Force control for planar spring-mass running *IEEE/RSJ Int. Conf. on Intelligent Robots and Systems (IROS)*
- [22] Hutter M *et al* 2010 SLIP running with an articulated robotic leg *IEEE/RSJ Int. Conf. on Intelligent Robots and Systems (IROS)*
- [23] Moore E Z 2002 Leg design and stair climbing control for the RHex robotic hexapod *Thesis* (McGill University)
- [24] Lin P C 2005 Proprioceptive sensing for a legged robot *Ph.D Dissertation* (Ann Arbor, MI: University of Michigan)
- [25] Burden S *et al* 2007 Heterogeneous leg stiffness and roll in dynamic running *IEEE Int. Conf. on Robotics and Automation (ICRA)*
- [26] Galloway K C *et al* 2011 Experimental investigations into the role of passive variable compliant legs for dynamic robotic locomotion *IEEE Int. Conf. on Robotics and Automation (ICRA)*
- [27] Bullimore S R and Burn J F 2006 Consequences of forward translation of the point of force application for the mechanics of running *J. Theor. Biol.* **238** 211–9
- [28] Spagna J C *et al* 2007 Distributed mechanical feedback in arthropods and robots simplifies control of rapid running on challenging terrain *Bioinspir. Biomim.* **2** 9–18
- [29] Rummel J and Seyfarth A 2008 Stable running with segmented legs *Int. J. Robot. Res.* **27** 919–34
- [30] Jun J Y and Clark J E 2011 Effect of rolling on running performance *IEEE Int. Conf. on Robotics and Automation (ICRA)*
- [31] Ankarali M M *et al* 2012 A dynamic model of running with a half-circular compliant leg *Int. Conf. on Climbing and Walking Robots (CLAWAR)*
- [32] Seipel J E and Holmes P 2007 A simple model for clock-actuated legged locomotion *Regular Chaotic Dyn.* **12** 502–20
- [33] Shen Z H and Seipel J E 2012 A fundamental mechanism of legged locomotion with hip torque and leg damping *Bioinspir. Biomim.* **7** 046010
- [34] Jun J Y and Clark J E 2012 A reduced-order dynamical model for running with curved legs *IEEE Int. Conf. on Robotics and Automation (ICRA)*
- [35] Huang K J and Lin P C 2012 Rolling SLIP: a model for running locomotion with rolling contact *IEEE/ASME Int. Conf. on Advanced Intelligent Mechatronics (AIM)*

- [36] Seyfarth A *et al* 2002 A movement criterion for running *J. Biomech.* **35** 649–55
- [37] Geyer H, Seyfarth A and Blickhan R 2005 Spring-mass running: simple approximate solution and application to gait stability *J. Theor. Biol.* **232** 315–28
- [38] McMahon T A 1975 Using body size to understand the structural design of animals: quadrupedal locomotion *J. Appl. Physiol.* **39** 619–27
- [39] McMahon T A and Cheng G C 1990 The mechanics of running: how does stiffness couple with speed? *J. Biomech.* **23** 65–78
- [40] Ghigliazza R M *et al* 2005 A simply stabilized running model *SIAM Rev.* **47** 519–49
- [41] Chou Y C *et al* 2012 Bio-inspired step-climbing in a hexapod robot *Bioinspir. Biomim.* **7** 036008
- [42] Heglund N C, Taylor C R and McMahon T A 1974 Scaling stride frequency and gait to animal size—mice to horses *Science* **186** 1112–3
- [43] Huang K J, Chen S C and Lin P C 2012 A bio-inspired single-motor-driven hexapod robot with dynamical gaits *IEEE/ASME Int. Conf. on Advanced Intelligent Mechatronics (AIM)*